Title: The double-edged role of nitric oxide drives predictable microbial community organization according to the microenvironment.

Steven A. Wilbert[1] and Dianne K. Newman[1,2,*]

Contact information:

[1] Division of Biology and Biological Engineering, California Institute of Technology, Pasadena, California, USA, 91125

[2] Division of Geological and Planetary Sciences, California Institute of Technology, Pasadena, California, USA, 91125

[*]**Correspondence:**

Dianne K. Newman

1200 E. California Blvd., Mail code 147-75

Pasadena, CA 91125

Telephone: 626-395-3543

Email: dkn@caltech.edu

Keywords: Polymicrobial communities, metabolism, metabolic cross-feeding, nitric oxide, nitrate, denitrification, spatial organization, microenvironment, oxygen gradients, *Pseudomonas aeruginosa*

Abstract

Microbial assemblages are omnipresent in the biosphere, forming communities on the surfaces of roots, rocks, and within living tissues. These communities can exhibit strikingly beautiful compositional structures, with certain members reproducibly occupying particular spatiotemporal microniches. Yet often, we lack the ability to explain the spatial patterns we see within them. To test the hypothesis that certain spatial patterns in microbial communities may be explained by the exchange of redox-active metabolites whose biological function is sensitive to environmental gradients, here we developed a simple community consisting of synthetic *Pseudomonas aeruginosa* strains with a partitioned denitrification pathway: a strict consumer and strict producer of nitric oxide (NO), a key pathway intermediate. Because NO can be both toxic or beneficial depending on the amount of oxygen present, this system provided an opportunity to investigate whether dynamic oxygen gradients can tune metabolic cross-feeding

in a predictable fashion. Using a combination of genetic analysis, different growth environments and imaging, we show that oxygen availability controls whether NO cross-feeding is commensal or mutually beneficial, and that this organizing principle maps to the microscale. More generally, this work underscores the importance of considering the double-edged roles redox-active metabolites can play in shaping microbial communities.

Introduction

Given the diversity of microbial metabolic strategies and that microbes rarely live alone, the potential for metabolic interactions is vast (Zuñiga et al., 2017). Metabolic interactions can be positive or negative and can have profound effects on the surrounding environment, from contributing to nutrient flux to stimulating the immune system of an infected animal or plant. Therefore, there is an increasing appreciation for the need to characterize and predict such interactions (Widder et al., 2016). Numerous ecological models have been developed to better understand how such interactions influence the growth and subsequent spatial patterning of a community (Goldford et al., 2018; Niehaus et al., 2019; Ratzke et al., 2020). However, these models typically focus on simple growth kinetics involving a shared or exchanged beneficial metabolite and do not consider how changing microenvironments over small spatial scales can influence the initiation and/or quality of interactions dependent upon this metabolite. In particular, dynamic spatiotemporal changes in oxygen availability is a well-documented ecological phenomenon microbes are confronted with (Dal Co et al., 2019; Krichels et al., 2019; Lowery and Ursell, 2019; Stewart et al., 2016), but is often overlooked in these models.

Diffusible, redox-active metabolites, be they organic or inorganic, are particularly interesting to consider in this context, as these molecules' reactivity is highly sensitive to local chemistry. Recent work has called attention to the fact that certain redox-active metabolites have the potential to be both toxic (i.e. generate reactive oxygen species under oxic conditions) or beneficial (i.e. contribute to energy conservation under anoxic conditions), thereby having the potential to play different and dynamic roles in the development of a microbial community (Dahlstrom et al., 2020). Such double-edged effects may be particularly important when the metabolite in question is an intermediate in a common metabolic pathway. For example, if two microbes are reliant on each other for growth due to an intermediate that can be toxic to the producer but is essential for the consumer, it stands to reason that their growth and subsequent environmental impact will depend on microenvironmental conditions that tune the properties of the exchanged intermediate. The potential for variable local interactions due to shifting

environmental gradients would therefore be expected to tune when, where, and how certain microbial interactions would manifest spatiotemporally.

As a step towards testing this general hypothesis, we sought to create a simple synthetic model system in which to explore the effect of the microenvironment on the interactions between two bacterial partners linked via an exchanged redox-active metabolite. Four criteria guided our development of such a system. First, we required that the metabolite be "agathokakological", a word derived from Greek roots meaning "composed of good and evil", in other words, a metabolite that is predictably "double-edged": beneficial or harmful according to its context. Second, we needed to be able to measure and perturb the most important environmental parameter—oxygen—that affects its physiological functions. Third, we aimed to control the production and utilization of this metabolite via the generation of mutant strains from an isogenic background in order to focus strictly on the capacity to make or use it. Finally, we sought a metabolic exchange that is broadly ecologically relevant across many environments.

The exchange of nitric oxide (NO) met all of our criteria. NO is known in both the eukaryotic and microbial worlds as a potent signaling molecule and a highly reactive nitrogen species that can damage a variety of cellular components (Volk et al., 2004). In the absence of oxygen, NO is toxic at high concentrations by antagonizing Fe-S centers and causing DNA damage; yet in the presence of oxygen, much lower levels of NO can be toxic due the generation of peroxynitrite; (Koppenol and Koppenol, 2021; Zumft, 1997). Microbes have numerous mechanisms to deal with low levels of NO toxicity such as flavohemoglobin proteins (Fhp) that can reduce NO to nitrous oxide (N_2O), or mediate its oxidation to nitrate (NO_3^-), depending on the environment (Arai, 2011; Koskenkorva et al., 2008), and other dioxygenases can sequester NO (Sasaki et al., 2016; Yoon et al., 2007). While NO has been studied in detail with respect to these properties, it can also support energy conservation. At the right concentrations, and if a microbe has the requisite machinery to process it, in the absence of oxygen, NO can serve as a terminal electron acceptor (TEA) for anaerobic respiration (Carr et al., 1989; Kalkowski, 1991). Yet as its concentration rises, and if producing cells or neighbors are unable to reduce it to nitrous oxide (N_2O), it reaches toxic levels and leads to local growth inhibition or death (Brunelli et al., 1995; Yu et al., 1999).

NO production is a landmark step in denitrification, where the soluble substrate nitrite (NO_2^-) is reduced to gaseous NO. Denitrification *sensu stricto* plays a critical role in the loss of nitrogen in soils (Fang et al., 2015; Krichels and Yang, 2019; Tian et al., 2019). If an organism contains a full pathway to sequentially reduce nitrate (NO_3^-) > NO_2^- > NO > N_2O > nitrogen gas (N_2), harmless N_2 will be released into the environment where it can eventually become recycled

102 by nitrogen fixing species (Kuypers et al., 2018). However, it is becoming more clear that the
103 complete reduction of nitrate to nitrogen gas may occur as a polymicrobial community effort in
104 which different members contain only a subset of the denitrification pathway (Gowda et al.,
105 2020; Hester et al., 2019; Lycus et al., 2017; Rich et al., 2003). Synthetic *Pseudomonas*
106 *aeruginosa* strains have been shown to exchange NO_2^- under strictly anoxic conditions, leading
107 to predictable spatial patterns that are sensitive to pH-dependent abiotic nitrite reduction to toxic
108 nitrogen species (Borer et al., 2020; Lilja and Johnson, 2016). In an independent study,
109 environmental isolates that naturally differed in their possession of denitrification genes were
110 used to create a model that predicted interactions via denitrification intermediates (Gowda et al.,
111 2020); yet, in this case, NO production was only considered for its potential toxicity rather than
112 its potential for energy conservation. Importantly, while older physiological studies have shown
113 that NO can support energy conservation as the sole terminal electron acceptor (Carr et al.,
114 1989; Voβwinkel et al., 1991), to our knowledge, the ability for NO to be exchanged between
115 cells in a manner that supports growth has not be demonstrated.
116 In this study, we utilized different mutant strains of the denitrifying organism, *P.*
117 *aeruginosa* strain PA14, to test the hypothesis that the spatial interactions of strains exchanging
118 NO can be predictably altered as a function of oxygen in the microenvironment. *P. aeruginosa* is
119 a cosmopolitan organism, notorious for being an opportunistic human pathogen, but also found
120 in sediments and soils (Arai, 2011). *P. aeruginosa* is also a classic denitrifier that encodes all
121 enzymes necessary for the complete reduction of nitrate to nitrogen gas and can be easily
122 genetically manipulated, permitting the creation of a synthetic NO cross-feeding community. Our
123 findings with this model community provide a conceptual lens through which to interpret more
124 complex microbial community patterning in nature and disease involving the exchange of
125 agathokakological metabolites.
126
127 **Results**
128 **Design and characterization of a synthetic NO cross-feeding community.**
129 The PA14 genome contains a full suite of respiratory enzymes for the complete
130 dissimilatory reduction of NO_3^- to N_2 (Nar, Nap, Nir, Nor, Nos) (Figure 1A) (Arai, 2011), and
131 previous studies have shown that these steps occur sequentially (Carlson and Ingraham, 1983).
132 Accordingly, we hypothesized that it would be possible to partition the PA14 denitrification
133 pathway between two strains, a NO producer and a NO consumer, to make a synthetic
134 community with the ability to catalyze the complete denitrification reaction (Figure 1B,
135 Supplementary file 1A). Several steps were necessary to construct a well-controlled system.

136 First, we generated a strain of PA14 lacking the nitrate reductase (Δ*narGHJI*, consumer 1,
137 Supplementary file 1A) and grew it in a rich medium anoxically in the presence of nitrate.
138 Compared to wild type PA (WT), growth without nitrate reductase was significantly slower
139 (Supplementary file 1B, orange line). Next, we generated a strain of PA14 lacking the nitric
140 oxide reductase (Δ*norCB*, producer 1; Supplementary file 1A); when grown under the same
141 conditions, this producer strain showed negligible growth (Supplementary file 1C, orange line).
142 This lack of growth was likely due to the reduction of nitrate to NO, which has been measured to
143 build up to 16μM in similar mutants, repressing nitrate reductase expression and preventing
144 further nitrate reduction as a survival mechanism (Yoon et al., 2007). When we mixed these two
145 strains in equal ratios (Supplementary file 1D, orange line), the mixture grew to a higher final
146 OD and nearly twice as fast as the consumer strain.
147 However, due to the sequential nature of the reduction steps, we realized it was possible
148 that the nitrate reductase mutant (consumer 1) strain could be reducing the NO_2^- intermediate
149 from the nitric oxide reductase mutant (producer 1) strain before NO was even generated (Lilja
150 and Johnson, 2016), or that the producer was benefiting from a secondary crosstalk via N_2O
151 reduction produced by the consumer (Supplementary file 1A, co-culture 1). To eliminate the
152 possibility of these unintended interactions, we removed the nitrite reductase (Nir) from the
153 consumer strain and the nitrous oxide reductase (Nos) from the producer strain (Supplementary
154 file 1A, co-culture 2). Growth of this new producer strain (Δ*norCB*Δ*nosZ*, producer 2) alone was
155 unchanged, indicating that NO growth inhibition or toxicity was still the primary phenotypic driver
156 (Supplementary file 1C, green line). The new consumer strain (Δ*narGHJI*Δ*nirS*, producer 2;
157 Supplementary file 1B, green line) lacking both the nitrate and nitrite reductases, however,
158 showed reduced growth compared to the nitrate-reductase only mutant (Supplementary file 1B,
159 orange line). When these two strains were grown together, there was still a rescue, although
160 slower (Supplementary file 1D, compare orange and green lines). We interpret this difference in
161 growth rate to be due to differential cross-feeding: 1) the strains only cross-feed NO (green
162 trace) or 2) the strains can cross-feed more than NO (yellow trace).
163 In experiments with our second set of co-culture strains (green), we noticed that the
164 consumer displayed reduced growth upon the removal of nitrite reductase, even though the
165 medium only contained added nitrate. This led us to speculate that the periplasmic nitrate
166 reductase (Nap) might be contributing to consumer growth, or at least reducing the nitrate
167 available to the producer; Nap is commonly thought to be used for redox balancing compared to
168 the membrane bound nitrate reductase (Nar), which contributes to proton translocation and
169 ultimately ATP generation (Richardson, 2000; Sparacino-Watkins et al., 2014; Van Alst et al.,

170 2009). To test this possibility, we generated a new set of partitioned strains (Supplementary file
171 1A, co-culture 3, 4), where Nap either was deleted from both the consumer and producer
172 (Δ*narGHJI*Δ*nirS*Δ*napAB*, co-culture 3, purple) or from the consumer only
173 (Δ*norCB*Δ*nosZ*Δ*napAB*, co-culture 4, red). In both cases (Supplementary file 1D) we observed
174 slightly faster growth for the third and fourth co-cultures compared to the second co-culture set,
175 likely due to the restriction of nitrate reduction by the most energetically favorable path (i.e. the
176 producer strain could only reduce nitrate via Nar). Based on these results, for the remainder of
177 our studies, we decided to further investigate the behavior of the nitric oxide producer
178 (Δ*norCB*Δ*nosZ*), consumer (Δ*narGHJI*Δ*nirS*Δ*napAB*), and co-culture described as co-culture 4
179 (hereafter referred to as the "co-culture") (Figure 1B,C).
180 To verify that the growth of the strains in the co-culture was due to the removal of NO
181 from the producer by the consumer, in a separate experiment, we functionally replayed the
182 consumer with the chemical NO scavenger, c-PTIO, growing the NO producer strain alone in its
183 presence or absence. In its absence, the producer failed to grow, consistent with the inhibitory
184 effect of NO accumulation. However, the addition of c-PTIO restored growth, supporting the
185 interpretation that NO reduction drives growth in the co-culture (Figure 1D).
186
187 **Single cell intermixing under planktonic and sessile anoxic conditions suggests NO**
188 **cross-feeding is mutually beneficial and proximity dependent.**
189 Because our planktonic growth experiments suggested there is a net community benefit
190 to strains in co-culture with a partitioned denitrification pathway under anoxic conditions (Figure
191 1C), we next sought to determine whether this reflected a mutual or commensal relationship. To
192 address this, we co-cultured and imaged strains expressing constitutive fluorescence markers
193 (GFP or mApple) after 2 days of growth. Population ratios indicated that both strains grew in the
194 co-cultures with the producer having a slight advantage likely due to its ability to continue
195 reducing nitrate (Supplementary file 2A). Swapping the fluorescent proteins between strains did
196 not change this outcome, indicating that this effect is specific to the denitrification effects and
197 not an artefact of GFP or mApple expression. These results suggest that this cross-feeding
198 interaction is mutual (the producer and the consumer represent approximately half of the total
199 population) in which the harm of NO to the producer is alleviated by the consumer, which, in
200 turn, gains an electron acceptor; together, the pathway can proceed.
201 Building on these results, we wondered how spatial structure might influence the growth
202 of the producer and consumer given that NO is a highly reactive and diffusible molecule. We
203 hypothesized that, unlike under shaken planktonic growth conditions in which the whole

204 population benefited, under spatially constrained anoxic conditions, proximity would determine
205 the success of community members. To test this prediction, we mixed fluorescently labeled cells
206 of the same or differing genotypes in equal ratios, and then diluted the cultures and sandwiched
207 them between a coverslip and a nitrate-supplemented agar medium pad such that single cells
208 were randomly distributed from one to dozens of cell lengths from each other. From these
209 starting positions, single cells could develop into aggregate biofilms over a 48-hour period.
210 Figure 2A graphically represents the strain mixtures shown in panel B as well as their predicted
211 interactions based on the results of our planktonic growth experiments. As controls, we mixed
212 WT with WT to explore how two cells with the full pathway and no growth defects would interact
213 under these conditions, as well as the consumer and producer strains with themselves. Finally,
214 the producer and consumer strains were mixed to visualize their interaction.
215 The two strains (GFP/mApple) in the WT mixture grew as large clonal expansions with
216 little single cell intermixing, indicating neither strain was impacted by the other (Ciccarese et al.,
217 2020; Weinstein et al., 2017). In contrast, the consumer mixture showed a dramatic reduction in
218 growth compared to WT, in line with the inability of these strains to reduce nitrate, a terminal
219 electron acceptor. The producer mixture, like the consumer mixture, showed a marked reduction
220 in individual aggregate growth, but also a reduction in total aggregates overall. We infer that the
221 producer strain likely was inhibited for growth but might also have been undergoing lysis. If we
222 compare the WT (Figure 2C) and co-culture (Figure 2D) under these conditions, most strikingly
223 we observe an increase in single cell intermixing between the two strains for the co-culture. The
224 two WT strains (GFP/mApple) appear to grow as clonal expansions, pushing against one
225 another rather than optimizing cell-cell contact. Conversely, the co-culture, although significantly
226 less dense than the WT mixture, appears to favor cell-cell contact between strains and form
227 mixed aggregates, suggestive of a mutual reliance on each other for continued growth. These
228 mixed aggregates were likely the result of close starting positions of producer and consumer
229 cells relative to one another.
230 In addition to intermixed co-culture aggregates, we also observed a difference in total
231 identifiable aggregates between single genotype mixtures and the co-culture. We observed few
232 producer-only aggregates when grown alone (Supplementary file 2B), likely due to growth
233 inhibition or toxicity of NO. However, when grown in co-culture, we observed an increase in
234 producer aggregate count across several fields of view (Supplementary file 2B). While
235 consumer-only aggregates were initially more numerous than producer-only aggregates
236 (compare Supplementary file 2C “Con” with 2B “Pro”), we found that co-culture with the
237 producer strain increased the variability of consumer aggregate count (Supplementary file 2C).

238 Importantly, reduction in total aggregates was observed owing to fields of view in which only one
239 intermixed co-culture aggregate was present. These results suggest that while single cell
240 intermixing can occur when the two strains are seeded at close initial starting positions (Figure
241 2D), NO may also diffuse outward from producer cell aggregates to reach consumer cells at
242 further distances, thereby increasing the interaction range. Together, these results extend our
243 planktonic growth observations into a spatial context, revealing how community members with a
244 partitioned denitrification pathway can interact under anoxic conditions where NO can diffuse.
245
246 **Oxygen availability induces synthetic community interaction and dials it from a**
247 **mutualistic (anoxic) to commensal (hyp(oxic)) interaction by increasing NO toxicity.**
248 Recognizing that many environments where denitrification occurs experience variable
249 amounts of oxygen, we wondered what would happen to NO reactivity and in the presence of
250 oxygen. Strains such as PA14 are facultative anaerobes, meaning they preferentially respire
251 oxygen when it is available (oxic conditions), but when oxygen is limited, they induce pathways
252 (such as the denitrification pathway) that permit energy conservation using alternative electron
253 acceptors. A classic example of this phenomenon is when cells grow planktonically but are not
254 shaken during growth. Cells at the surface of the medium reduce oxygen faster than it can
255 diffuse into the medium, resulting in an oxygen gradient (Price-Whelan et al., 2007). To expand
256 our understanding of when, where and how NO-cross feeding operates, we exploited this
257 phenomenon and measured growth in shaking or standing "oxic" cultures. We hypothesized
258 strains harboring a partitioned denitrification pathway would exhibit different behaviors
259 depending on the amount of oxygen and nitrate present, in a manner reflecting the
260 agathokakological effects of oxygen and NO on cells.
261 To test this hypothesis, we tracked the growth of different producer and consumer
262 strains, alone and in combination, over 48-hours in a continuously shaking plate reader to
263 prevent an oxygen gradient from forming. In the absence of nitrate all strains grew similarly, as
264 expected, indicating the genetic modifications had no off-target effects (Figure 3A). Conversely,
265 when we added 5 mM nitrate to the medium, the consumer strain slightly decreased its growth
266 compared to the WT and the producer strains displayed a brief growth arrest midway through
267 exponential phase, with growth then paralleling that seen for the WT or mixed producer +
268 consumer cultures (Figure 3B). Despite continuous shaking, at these cell densities, we surmise
269 from prior work that these strains began to experience oxygen-limitation during mid exponential
270 phase (Price-Whelan et al., 2007).

271 To induce hypoxic conditions in a way that oxygen concentration could be measured, we
272 performed the same growth experiment in a plate reader without shaking, thus inducing an
273 oxygen gradient. Again, in the absence of nitrate we did not see a difference between the
274 strains (Figure 3C). However, in the presence of nitrate, growth of the producer and consumer
275 individually slowed compared to the WT but was rescued in co-culture (Figure 3D). Importantly,
276 even without the ability to reduce nitrate, the consumer was able to reach the same final OD as
277 WT, suggesting that while its growth was slowed, it was able to overcome its inability to utilize
278 nitrate as a terminal electron acceptor under these conditions. Conversely, the producer
279 strain(s) showed a dramatic decrease in OD later in the growth curve, suggestive of cell lysis.
280 To validate that an oxygen gradient had formed over time, we used microelectrodes to profile
281 oxgyen concentrations throughout the depth of standing cultures for both WT and the co-culture
282 (Figure 3E).
283 NO will readily react with superoxide (O_2^-) to form the reactive nitrogen species,
284 peroxynitrite ($ONOO^-$). O_2^- is a by-product and intermediate of oxygen respiration which is
285 removed by superoxide dismutase (SOD), and $ONOO^-$ can out compete superoxide for SOD
286 leading to an accumulation of reactive oxygen species and oxidative stress (Brunelli et al.,
287 1995). Thus, we reasoned that the lysis we observed under hypoxic conditions might be
288 correlated with an increased production of superoxide. To test this idea, we used an intracellular
289 NO sensitive dye (DAF-2DA, Figure 3G) and a superoxide sensitive dye (CellROX, Figure 3F) to
290 detect these metabolites. Both NO and superoxide increased over the growth curve in the
291 producer strain alone (Figure 3F,G), with a rise in signal around 30 hours, correlating with the
292 drop in OD (Figure 3D, arrows, “lysis”).
293
294 **Differences in the transcriptional regulation of nitrate reductases leads to spatiotemporal**
295 **control of NO production during aggregate biofilm development.**
296 Based on the observation that the producer’s growth and self-toxicity was correlated with
297 oxygen availability, and because oxygen gradients like those seen in standing cultures (Figure
298 3E) readily form in biofilm contexts (Arshad et al., 2014; Spero and Newman, 2018; Stewart et
299 al., 2016), we next sought to visualize lysis as a spatial proxy for NO production. To achieve
300 this, we grew diluted cells on agar pads under oxic conditions to form aggregate biofilms,
301 focusing only on NO producing cells. Recalling that the substrate for the nitrite reductase that
302 produces NO can be generated by both Nap and Nar, we compared two different producer
303 strains, one that contained both Nap and Nar and one that only contained Nar (Figure 4A).
304 Because *nap* and *nar* genes are regulated by different transcription factors: *nap* by RpoS

305 (stationary phase/quorum sensing) (Schuster et al., 2004) and *nar* by ANR (nitrate and low
306 oxygen) (Arai, 2011), we hypothesized that NO production in aggregate biofilm might be a
307 differential spatial distributed as a function of the strain's genomic content and thus
308 transcriptional regulation.
309 Inoculated agar pads were pre-incubated at 37°C under oxic conditions for 18 hours to
310 enable aggregate biofilm development after which we performed time lapse imaging at 37°C to
311 track subsequent growth and lysis. The producer containing both Nap and Nar grew into overall
312 smaller aggregate biofilms compared to the producer containing Nar only before undergoing a
313 wave of lysis starting at the periphery and moving inward (Figure 4B). High magnification views
314 of lysis illustrate that cells no longer appear black under phase and no longer contain
315 fluorescence (Supplementary file 4A). It is possible that the pattern of lysis observed in the
316 biofilms reflects relatively more NO being made by peripheral cells that have greater access to
317 oxygen and nutrients (Smriga et al., 2021); by the same token, these cells are the first to
318 experience NO-induced toxicity and die. To test this idea, we used the oxidative stress
319 fluorescent probe, CellROX on similar biofilms (containing both Nap and Nar) to visualize local
320 toxicity in relation to cell lysis. Though our planktonic experiments successfully documented a
321 correlation between superoxide and NO production with fluorescent probes (Fig. 3F, 3G), the
322 NO probe was too dim to quantify relative to the autofluorescent background, thus superoxide
323 detection is our proxy for NO. We observed a strong correlation between CellROX intensity
324 patterns and lysis, reinforcing that oxidative stress begins at the periphery and moves towards
325 the center as lysis progresses (Fig. 4D, 4E). Such peripheral death would collapse an oxygen
326 gradient, resulting in a lysis cascade as deeper cells continue to produce NO now in the
327 presence of more oxygen until all cells have lysed.
328 Conversely, the producer that only contains Nar initially develops into large aggregate
329 biofilms, likely due to little NO production until Nar is activated in response to low oxygen in the
330 interior and the presence of nitrate, leading to internal NO production and lysis (Figure 4C).
331 Interestingly, when we compared CellROX staining of three different producer (Nar) biofilms at
332 different stages of lysis, we also saw a dramatic increase in staining that started centrally and
333 worked its way outward. These results give credence to our model, but also indicate that lysis at
334 the perimeter or core are both due to oxidative stress. This could either be due to trace oxygen
335 being present in the core initially, allowing superoxide production, or anoxic NO buildup
336 inhibiting metabolism, thereby causing a collapse of the oxygen gradient.
337
338 **Microenvironmental control of NO cross-feeding leads to predictable spatial patterns.**

339 To visualize dynamic interactions between NO producers and consumers, we again
340 mixed the strains with themselves or each other and incubated them under oxic conditions on
341 nutrient agar pads containing nitrate. After 24 hours of growth, we observed that WT, like under
342 anoxic conditions, grew into aggregate biofilms, but rather than as monolayers, these biofilms
343 appeared thicker, perhaps due to the ability to support oxic and anoxic growth (Figure 5A). The
344 consumer mixture also grew into large aggregate biofilms (much larger than under anoxic
345 conditions due to its access to oxygen as a TEA), though the expansions were not as dense
346 due to the inability to support anoxic growth with nitrate (Figure 5A). The producer only mixture
347 again showed lysis (Figure 5A). Strikingly, the border between the the producer and consumer
348 in co-culture was dramatically different.
349 As seen under anoxic conditions (Figure 2C), WT strains showed no intermixing,
350 suggestive of no interaction/advantage or reliance on each other (Figure 5B). The co-culture,
351 however, showed lysis of producer cells when not in proximity to consumer cells and an
352 increase in single cell intermixing (Figure 5C). This suggests that from the beginning, the co-
353 culture single cells grew into clonal expansions, not interacting until the microenvironment was
354 metabolically altered (depletion of oxygen, beginning utilization of nitrate); the producer began
355 to lyse on its own, but when in proximity to a consumer, was relieved of NO toxicity. In other
356 words, over time, metabolic dynamics unlock a spatial niche where cross-feeding provides a
357 selective advantage. Such protection manifested in several ways (Figure 5D): some producer
358 cells appeared to cling to the consumer cells, following their contour; other producer cells
359 appeared to be protected by a pocket formed by consumer cells; and still others were protected
360 by regions of high intermixing. Knowing that the producer cells would lyse without local NO
361 depletion (Figure 4) permits us to link cellular spatial arrangement to physiological activity. To
362 further test this interpretation, we set up additional pads with the co-culture, pre-incubating them
363 until just before the producer showed lysis, and recording the cellular dynamics over time. As
364 predicted, the producer (Nap/Nar) cells lysed; however, unlike when grown alone where lysis
365 began at the periphery (compare to Figure 4B), the producer in the co-culture experiment
366 showed lysis beginning several cell lengths from the periphery when in close proximity to
367 consumer strains (Figure 5E).
368 Interestingly, in contrast to mixtures using the Nap/Nar producer (Supplementary file
369 4A), when the same experiment is performed using the producer that only contains Nar, rescue
370 of the producer is not observed by the consumer, presumably due to NO only being generated
371 in the biofilm core, too far from the consumer to trigger a mutually-beneficial interaction
372 (Supplementary file 4B). These results suggest a model in which initially the two strains do not

interact because they have full access to oxygen and do not yet need nitrate. However, as they grow larger and an oxygen gradient forms in the microenvironment, the producer begins generating NO which leads to self-lysis unless the producer is proximal to the consumer, which relieves the producer's self-toxicity and provides the consumer a terminal electron acceptor (Supplementary file 4C).

Discussion

Microbial metabolism is increasingly appreciated for its contributions to human and environmental health (Hester et al., 2019; Ponomarova and Patil, 2015; Zuñiga et al., 2017), and awareness of the diversity of microbial metabolic interactions is expanding with improved techniques for identifying new pathways and observing interactions (Cordero and Datta, 2016; Dar et al., 2021; DePas et al., 2016; Pessi et al., 2020; Wilbert et al., 2020; Zuñiga et al., 2017). In the face of this progress, gaining a better understanding of how these interactions may shift as a function of dynamic oxygen gradients is an important goal. We developed a synthetic microbial community linked by the exchange of NO, an agathokakological molecule whose biological effects are tuned by the presence of oxygen, as a step towards this end. Our work shows that the interactions that drive NO intercellular exchange and reduction are induced and sensitive to the genetic content of community members and microenvironmental gradients, knowledge of which leads to predictable organizational outcomes.

Differential regulation of the Nar and Nap enzymes, both of which produce nitrite, the metabolic precursor of NO in the denitrification pathway, directly impacts NO producer and consumer interactions. Nar is induced under anoxic conditions and contributes to energy conservation (Arai, 2011) whereas Nap can be expressed in (hyp)oxic environments and facilitates redox balancing (Brondijk et al., 2004; Gates et al., 2008). These differences in regulation thereby control NO production and reduction across a range of oxygen regimes. Linking metabolic interactions to microscale microbial organizations is an important and increasingly appreciated goal (Fuhrman, 2009; Gralka et al., 2020; Kuhns et al., 2015; Ma and Cordero, 2018; Proctor and Relman, 2017; Widder et al., 2016). That genomic content—including regulatory structure—shapes microbial interactions is not surprising, yet the point that differential regulation of key steps in a partitioned metabolic pathway can determine interaction outcomes is important to keep in mind when attempting to understand and predict when and how members of complex microbial communities may spatially associate.

Our findings spotlight local oxygen availability for its ability to tune both the nature and need for a cross-feeding relationship. In our example case, NO can generate toxic byproducts in

407 the presence of oxygen, leading to cellular growth arrest. Yet in the absence of oxygen, NO can
408 be a lifeline, serving as a terminal electron acceptor and promoting energy conservation and
409 growth. These agathokakological effects are important because oxygen is often
410 heterogeneously available in natural systems, exhibiting steep environmental gradients over
411 small spatial scales (Kolpen et al., 2014; Krichels et al., 2019). Because of this, oxygen
412 availability influences whether strains with a bifurcated denitrification pathway exhibit mutualism
413 (in anoxic environments, growth of the NO producer and consumer is co-dependent) or
414 commensalism (in (hyp)oxic environments, growth of the NO producer is constrained due to
415 toxicity in the absence of the consumer, whereas the consumer does not rely on NO to support
416 growth). Moreover, oxygen gradients can shape microbial interactions both in planktonic and
417 sessile communities, with the scales over which these interactions occur being set by the
418 proximity of interacting cells and their local microenvironment, which they in turn alter in space
419 and time.

420 While our work with a well-controlled synthetic community allowed us to make these
421 observations, an important next step will be to determine whether mixtures of natural isolates
422 with partitioned metabolic pathways play by the same rules. Our work gives rise to testable
423 predictions about when and where NO cross-feeding may occur. For example, it is well
424 appreciated that NO is an important intermediate species in the nitrogen cycle (Kuypers et al.,
425 2018), whose turnover rates may decide the fate of soil nitrogen stores. Interestingly, recent
426 metagenomic studies indicate that within certain habitats, there an enrichment for organisms
427 that can only reduce NO to N_2O, an important greenhouse gas (Pessi et al., 2020). Thus, an
428 understanding what constrains NO reduction may provide insight into a metabolic process with
429 important environmental consequences. Recent studies have drawn attention to the potential for
430 partitioned pathways to influence the rate of nitrogen flux in soils by resident microbes (Gowda
431 et al., 2020; Pessi et al., 2020). Our work attempts to directly link structure and function of such
432 partitions as is suggested by the genomic content of environmental isolates (Pessi et al., 2020).
433 In an entirely different context, our finding that *P. aeruginosa* can thrive by reducing NO
434 provided by another cell lends credence to the hypothesis that PA may survive the host immune
435 NO attack by its reduction to N_2O, and may correlate with the appearance of N_2O in the breath
436 gas of cystic fibrosis patients (Kolpen et al., 2014). Importantly, *P. aeruginosa* can be found
437 proximal to host immune cells in these infected environments (DePas et al., 2016).

438 Finally, we note that NO is only one of many agathokakological molecules, both organic
439 and inorganic, that may help structure microbial communities over small spatial scales as a
440 function of oxygen availability. For example, other redox-active metabolites such as phenazines

441 can function as natural toxins or beneficial agents of nutrient acquisition and/or redox
442 homeostasis, depending on the microenvironmental context (Dahlstrom et al., 2020). Similarly,
443 sulfide has long been known to play nuanced roles in nature, with its concentration-dependent
444 toxicity influencing which phototrophic species are able to thrive (Findlay et al., 2015), and
445 where different energy-conserving processes can occur within microbial mats (Jungblut et al.,
446 2016; Prieto-Barajas et al., 2018). We hasten to note that many other parameters may be
447 subject to similar dynamic spatiotemporal gradients, such as carbon, pH and light, and are likely
448 to also play important roles in determining the niches where cross-feeding or other types of
449 metabolic interactions can occur (Zhang et al., 2021). Towards the goal of gaining a predictive
450 understanding of why diverse microbial communities are structured the way they are, a
451 constructive next step will be to model these interactions, iterating with experiments until cross-
452 cutting principles can be identified with predictive power.
453
454 **Materials and methods**
455 **Bacterial strains and growth conditions.** All strains used are clean deletion mutants
456 originating from the wild-type (WT) *Pseudomonas aeruginosa* UCBPP-PA14 strain as described
457 below. Strains were stored as 50% glycerol stocks at -80°C. Before use, strains were streaked
458 from frozen stock onto Bacto agar (BD, Sigma) plates containing LB (Miller, BD, Sigma) or LB
459 supplemented with 50ug/mL gentamicin (GoldBio) to select for retention of expression cassettes
460 within fluorescent strains, and grown overnight at 37°C. From streak plates, a dab of culture was
461 used to inoculate 5mL liquid cultures in LB or LB plus 50ug/mL gentamicin liquid media.
462 Cultures were shaken at 250rpm at 37°C overnight until fully saturated at stationary phase. To
463 standardize inoculum sizes between strains, each strain's optical density (OD_{500nm}) was
464 measured by spectrophotometry (Beckman Coulter). Strains were then each washed and
465 diluted to an OD of 1 via centrifugation and resuspension in 1X phosphate buffered saline
466 (PBS). Strains were then either further diluted directly, or first mixed at equal ratios for co-
467 culture experiments. For all experiments, we used a Low Salt LB (LSLB) in place of standard LB
468 powder due to microelectrode reactivity to high NaCl in LB. The composition of LSLB is 141mM
469 Tryptone (BD, Sigma), 16mM Yeast Extract (BD, Sigma), 45mM NaCl (Fisher Chemical), which
470 were dissolved in Mili-Q water and autoclaved. 5mM Nitrate was supplemented into LB or LSBL
471 where indicated by diluting from a 1M stock of KNO_3 (Fisher Chemical).
472
473 **Construction of mutant bacterial strains.** Table S1 contains a full list of primers used in the
474 creation of deletion constructs and mutant strains used in this study. Briefly, a 1kb fragment up-

475 and downstream of the target gene was amplified via PCR and cloned into the pMQ30 plasmid
476 using Gibson cloning (NEB) and transformed into *E. coli* cells as previously described (Spero
477 and Newman, 2018). Deletion constructs were then introduced to parent strains (WT PA14 and
478 or deletion strains of PA14, see Table S1) via triparental conjugation. *E. coli* plasmid and helper
479 strains were selected against by bead plating conjugation onto VBMM plates containing
480 50ug/mL gentamicin (Choi and Schweizer, 2006). Clean deletion strains were then bead plated
481 on a 10% sucrose plate to induce homologous recombination with the construct containing the
482 regions up- and downstream, but lacking the targeted gene locus (Basta et al., 2017). Mutant
483 strains were confirmed first by patching on sucrose and gentamicin plates, and successful
484 mutants grew on sucrose but not gentamicin. Next, PCR genotyping was performed using
485 primers that span the deletion region, sequencing confirmed the identity of these deletions, and
486 anaerobic growth challenges revealed expected physiological effects (e.g. ∆nirS was unable to
487 grow on nitrite, etc). Fluorescence strains were created as previously describe (Basta et al.,
488 2017; Meirelles and Newman, 2018) using fluorescent GFP/mApple plasmids driven by the
489 constative ribosomal promoter rpsG introduced into the Tn7 site of specified strains using tetra-
490 parental conjugation. *E. coli* helper strains were again selected against using VBMM containing
491 50ug/mL gentamicin. Confirmation of insertion was performed via microscopy, visualizing
492 colonies in both green and red fluorescence channels and selecting those that were bright in
493 their respective channel. Frozen stocks were also used to start cultures and image single cells
494 which showed significant fluorescence in appropriate channels above background
495 autofluorescence.
496
497 **Growth curves.** Anoxic growth curve media was placed in anaerobic chamber 72 hours prior to
498 experiment to allow time for oxygen to degas from media. 1 OD_{500nm} cultures were brought into
499 chamber and further diluted to 0.005 OD_{500nm} in anoxic media. Growth curves were performed
500 using a BioTek Synergy 4 plate reader stored in an anoxic chamber and set to 37C with shaking
501 and measured OD_{500nm} every 10 minutes. Oxic (shaking) and Hypoxic (stationary) growth curves
502 were set up as above but under normal atmosphere. Oxic growth curves were performed using
503 a Tecan Spark 10M set to orbital shaking. Hypoxic growth curves were performed using a
504 Spectramax M3 (Molecular Devices) plate reader set to not shake. Each condition was
505 performed in technical triplicate or quadruplicate. Each well contained 200 µl of culture with
506 40uL of mineral oil added to the top of each well to prevent evaporation of 48-72-hour growth
507 curves. Traces from all growth curves (Figure 1, Figure 3, Supplementary file 1) were analyzed

508 by plotting mean OD_{500nm} over time (dark center line) as well as 95% confidence intervals from
509 the technical replicates (shaded area) using Seaborn plotting packages in Python.
510
511 **Nitric oxide and superoxide quantification.** Levels of nitric oxide and superoxide were
512 quantitated using fluorescent dyes during hypoxic growth curves. NO was quantitated using
513 50μM DAF-2DA (Calbiochem, Sigma) which is internalized by cells where esterases free DAF-
514 2DA to interact with NO producing a green fluorescence signal (Aakanksha Wany, Pradeep
515 Kumar Pathak, 2020). Superoxide was quantitated using 5μM CellROX Deep Red (Thermo),
516 which is non-fluorescent in a reduced state but exhibits a strong induction of fluorescence upon
517 oxidation with reactive oxygen species (McBee et al., 2017). To measure these probes, a
518 hypoxic growth curve in LSLB with or without 5mM KNO_3 was performed as indicated above
519 and the Spectramax plate reader was configured to additionally measure green fluorescence
520 (Ex. 488nm, Em. 520nm, DAF-2) and far red fluorescence (Ex. 640nm, Em. 665nm, CellROX).
521 For pad imaging assays, CellROX was supplemented to the agar pads directly at a final
522 concentration of 10μM and imaged after significant biofilm growth had occurred to reveal
523 superoxide localization. DAF-2DA was also used to visualize NO, however, due to weak single-
524 cell signal and strong background autofluorescence in the green channel, we were unable to
525 visualize the signal.
526
527 **Oxygen profiling.** To confirm the presence of oxygen gradients in standing cultures, we
528 employed a 25μm diameter oxygen microelectrode electrode (Unisense), which was calibrated
529 as previously described (Spero and Newman, 2018). Briefly, LSLB media incubated at 37°C
530 was used to calculate the high point O_2 concentration. A zero-point calibration was obtained by
531 dissolving 2g Sodium Ascorbate in 100mL 0.1 NaOH, which scavenges O_2 from the medium.
532 Using the Unisense Sensor Suite Software to save calibration values and to control a motorized
533 micromanipulator to perform profiling, O_2 was measured from the surface of hypoxically
534 incubated planktonic cultures in 1mL Eppendorf tubes. The surface was set by eye and
535 confirmed by a reduction in mV signal. O_2 was then measured over a 1mm distance below the
536 surface at 50μm intervals. Two measurements were taken at each position, and three technical
537 replicates were averaged and displayed as the mean value with 95% confidence intervals
538 (Figure 3E). Cultures were prepared as in growth curves but maintained as 1mL volumes in
539 tubes rather than aliquoting into 96-well plates. Mineral oil was not added due to potential
540 incompatibility with electrodes.
541

542 **Agar pad imaging assay.** After significant optimization, it was determined that 1 OD_{500nm}
543 cultures diluted to a starting concentration of 0.001 OD_{500nm} was sufficient to obtain single cells
544 randomly distributed under agar pads. Agar pads were made by combining LSLB media with or
545 without 5mM KNO_3, with 2% w/v Noble Agar (BD, Sigma). Prior to use, the agar was melted by
546 microwaving. To make equally sized agar pads, 100µL was pipetted into each of several square
547 molds (6-7mm X 7mm X 1.6mm Depth ID, 25mm X 75mm, Grace Bio Labs), placed between
548 two glass microscope slides, and allowed to solidify at 4°C until use. Anoxic pads were made 72
549 hours in advance and placed in an anaerobic chamber to degas. 5 µL of 0.001 OD_{500nm} dilution
550 culture was added to the bottom of a well in an 8-well LabTek dish (Thermo). An agar pad was
551 then placed on top of the culture. LabTek cultures were incubated at 37°C for 24 hours (oxic) or
552 48 hours (anoxic) in a sealed container (6.7ounce, Systema). Importantly, when additional
553 humidity was added using a wet tissue under samples, instead of distinct aggregate biofilms,
554 cells grew more like intermixed planktonic cultures; thus, additional humidity was not added.
555 Time lapse imaging of pads was performed by first incubating pads as described above, but just
556 before lysis would occur (empirically determined to be at approximately 18 hours), LabTek
557 cultures were sealed with parafilm to prevent evaporation in the heated microscope incubation
558 chamber. Anoxically-incubated cells were not initially fluorescent upon removal from chamber to
559 image due to an inability for fluorophores to fold in the absence of oxygen. To overcome this,
560 pads were placed at 4ºC without lids for one to two hours prior to imaging which resulted in
561 sufficient signal recovering to differentiate between GFP and mApple cells.
562
563 **Imaging and image analyses.** All imaging was performed using a Nikon Ti2 widefield
564 fluorescence microscope. End time point images were collected using a Plan Fluor 100x/1.30 oil
565 phase objective and time lapse images were collected using a Plan Apo 40x/0.90 dry phase
566 objective. GFP channel used a 488nm LED excitation light source and emission was collected
567 with a FITC filter. The mApple channel used 561nm LED light source and emission was
568 collected with a TRITC filter. For time lapse imaging, an OKO Labs cage incubation unit was set
569 to 37°C several hours before imaging to equilibrate the microscope stand and used for the
570 duration of the imaging experiment. Images were collected every 20 minutes from multiple stage
571 positions. Time indicated in figures (Figure 4B,C, Figure 5E) represents time since the pads
572 were inoculated. Images were analyzed and prepared for display using FIJI (Schindelin et al.,
573 2012). Anoxically-incubated cells showed significantly less fluorescence than oxically incubated
574 ones; in order to optimally observe cells over background, a background subtraction using FIJI's
575 built-in function was performed. Brightness and contrast were adjusted on a per image basis in

576 order to best display cell positions and identifications, unless otherwise noted (e.g. CellROX
577 intensity in biofilms imaged and displayed the same for comparison of intensity (Figure 4D)). To
578 account for significant drift of the agar pads during time lapse imaging and produce the videos
579 and montages displayed herein, an image registration was performed using the StackReg
580 plugin with the Rigid Body choice. Image segmentation was used to quantify the ratio of
581 GFP:mApple cells in the anoxic planktonic cultures (Supplementary file 2A),. Briefly, contrast
582 was enhanced, background subtracted fluorescence channels were combined to create a total
583 cell mask. The Auto local Threshold function with the Phansalkar selection was used to
584 segment and count both the total and GFP channel cells. Because cells appeared to become
585 more fluorescent in the mApple channel during long anoxic incubations, this prevented us from
586 being able to segment mApple cells directly. Therefore, we calculated mApple cell counts as
587 total cell counts minus GFP cell counts, then used these values to compute population
588 percentages.
589
590 **Acknowledgments.** The work was supported by the National Institutes of Health
591 (R01HL152190 to D.K.N.) and the National Science Foundation Graduate Student Fellowships
592 Program (to S.A.W.). We would like to thank the current and past Newman Lab members for
593 feedback and discussions. Specifically, we thank Drs. Darcy McRose and Avi Flamholz for
594 critical manuscript review, Dr. Melanie Spero for molecular technique instruction, Drs. Reinaldo
595 Alcade and Georgia Squyres for fruitful discussion and troubleshooting imaging assays, and Dr.
596 Michael Piacentino for help with coding and general morale.
597
598 **Competing interests.** The authors declare no conflict of interests.
599

References

Aakanksha Wany, Pradeep Kumar Pathak and KJG. 2020. Methods for Measuring Nitrate Reductase, Nitrite Levels, and Nitric Oxide from Plant Tissues Aakanksha **2057**:5–6.

Arai H. 2011. Regulation and Function of Versatile Aerobic and Anaerobic Respiratory Metabolism in Pseudomonas aeruginosa. *Front Microbiol* **2**:103. doi:10.3389/fmicb.2011.00103

Arshad TA, Bonnecaze RT, Shear JB, Whiteley M, Wessel AK, Connell JL, Fitzpatrick M. 2014. Oxygen Limitation within a Bacterial Aggregate. *MBio* **5**. doi:10.1128/mbio.00992-14

Basta DW, Bergkessel M, Newman DK. 2017. Identification of fitness determinants during energy-limited growth arrest in Pseudomonas aeruginosa. *MBio* **8**:1–17. doi:10.1128/mBio.01170-17

Borer B, Ciccarese D, Johnson D, Ori D. 2020. Spatial organization in microbial range expansion emerges from trophic dependencies and successful lineages Benedict. *Commun Biol* 1–10. doi:10.1038/s42003-020-01409-y

Brondijk THC, Nilavongse A, Filenko N, Richardson DJ, Cole JA. 2004. NapGH components of the periplasmic nitrate reductase of Escherichia coli K-12: Location, topology and physiological roles in quinol oxidation and redox balancing. *Biochem J* **379**:47–55. doi:10.1042/BJ20031115

Brunelli L, Crow JP, Beckman JS. 1995. The comparative toxicity of nitric oxide and peroxynitrite to escherichia coli. *Arch Biochem Biophys*. doi:10.1006/abbi.1995.1044

Carlson CA, Ingraham JL. 1983. Comparison of denitrification by Pseudomonas stutzeri, Pseudomonas aeruginosa, and paracoccus denitrificans. *Appl Environ Microbiol* **45**:1247–1253. doi:10.1128/aem.45.4.1247-1253.1983

Carr GJ, Page MD, Ferguson SJ. 1989. The energy-conserving nitric-oxide-reductase system in Paracoccus denitrificans Distinction from the nitrite reductase that catalyses synthesis of nitric oxide and evidence from trapping experiments for nitric oxide as a free intermediate during denitrifi. *Eur J Biochem* **179**:683–692. doi:10.1111/j.1432-1033.1989.tb14601.x

Choi KH, Schweizer HP. 2006. mini-Tn7 insertion in bacteria with single attTn7 sites: Example Pseudomonas aeruginosa. *Nat Protoc* **1**:153–161. doi:10.1038/nprot.2006.24

Ciccarese D, Zuidema A, Merlo V, Johnson DR. 2020. Interaction-dependent effects of surface structure on microbial spatial self-organization. *Philos Trans R Soc B Biol Sci* **375**:20190246. doi:10.1098/rstb.2019.0246

Cordero OX, Datta MS. 2016. Microbial interactions and community assembly at microscales. *Curr Opin Microbiol* **31**:227–234. doi:10.1016/j.mib.2016.03.015

634 Dahlstrom KM, McRose DL, Newman DK. 2020. Keystone metabolites of crop rhizosphere
635 microbiomes. *Curr Biol* **30**:R1131–R1137. doi:10.1016/j.cub.2020.08.005
636 Dal Co A, Ackermann M, van Vliet S. 2019. Metabolic activity affects response of single cells to
637 a nutrient switch in structured populations. *bioRxiv*. doi:10.1101/580563
638 Dar D, Dar N, Cai L, Newman DK. 2021. In situ single-cell activities of microbial populations
639 revealed by spatial transcriptomics. *bioRxiv* 2021.02.24.432792.
640 DePas WH, Starwalt-Lee R, Van Sambeek L, Kumar SR, Gradinaru V, Newman DK. 2016.
641 Exposing the three-dimensional biogeography and metabolic states of pathogens in cystic
642 fibrosis sputum via hydrogel embedding, clearing, and rRNA labeling. *MBio* **7**:1–11.
643 doi:10.1128/mBio.00796-16
644 Fang Y, Koba K, Makabe A, Takahashi C, Zhu W, Hayashi T, Hokari AA, Urakawa R, Bai E,
645 Houlton BZ, Xi D, Zhang S, Matsushita K, Tu Y, Liu D, Zhu F, Wang Z, Zhou G, Chen D,
646 Makita T, Toda H, Liu X, Chen Q, Zhang D, Li Y, Yoh M. 2015. Microbial denitrification
647 dominates nitrate losses from forest ecosystems. *Proc Natl Acad Sci U S A* **112**:1470–
648 1474. doi:10.1073/pnas.1416776112
649 Findlay AJ, Bennett AJ, Hanson TE, Luther GW. 2015. Light-dependent sulfide oxidation in the
650 anoxic zone of the chesapeake bay can be explained by small populations of phototrophic
651 bacteria. *Appl Environ Microbiol* **81**:7560–7569. doi:10.1128/AEM.02062-15
652 Fuhrman JA. 2009. Microbial community structure and its functional implications. *Nature*
653 **459**:193–199. doi:10.1038/nature08058
654 Gates AJ, Richardson DJ, Butt JN. 2008. Voltammetric characterization of the aerobic energy-
655 dissipating nitrate reductase of Paracoccus pantotrophus: Exploring the activity of a redox-
656 balancing enzyme as a function of electrochemical potential. *Biochem J* **409**:159–168.
657 doi:10.1042/BJ20071088
658 Goldford JE, Lu N, Bajić D, Estrela S, Tikhonov M, Sanchez-Gorostiaga A, Segrè D, Mehta P,
659 Sanchez A. 2018. Emergent simplicity in microbial community assembly. *Science (80-)*
660 **361**:469–474. doi:10.1126/science.aat1168
661 Gowda K, Ping D, Mani M, Kuehn S. 2020. A sparse mapping of structure to function in
662 microbial communities. *bioRxiv* 1–16.
663 Gralka M, Szabo R, Stocker R, Cordero OX. 2020. Trophic Interactions and the Drivers of
664 Microbial Community Assembly. *Curr Biol* **30**:R1176–R1188.
665 doi:10.1016/j.cub.2020.08.007
666 Hester ER, Jetten MSM, Welte CU, Lücker S. 2019. Metabolic overlap in environmentally
667 diverse microbial communities. *Front Genet* **10**:1–10. doi:10.3389/fgene.2019.00989

668 Jungblut AD, Hawes I, Mackey TJ, Krusor M, Doran PT, Sumner DY, Eisen JA, Hillman C,
669 Goroncy AK. 2016. Microbial mat communities along an oxygen gradient in a perennially
670 ice-covered Antarctic lake. *Appl Environ Microbiol* **82**:620–630. doi:10.1128/AEM.02699-15
671 Kalkowski I. 1991. Metabolism of nitric oxide in denitrifying Pseudomonas aeruginosa and
672 nitrate-respiring Bacillus cereus. *FEMS Microbiol Lett* **82**:107–112. doi:10.1016/0378-
673 1097(91)90429-E
674 Kolpen M, Kühl M, Bjarnsholt T, Moser C, Hansen CR, Liengaard L, Kharazmi A, Pressler T,
675 Høiby N, Jensen PØ. 2014. Nitrous oxide production in sputum from cystic fibrosis patients
676 with chronic Pseudomonas aeruginosa lung infection. *PLoS One* **9**.
677 doi:10.1371/journal.pone.0084353
678 Koppenol H, Koppenol H. 2021. Nitric oxide, superoxide, and peroxynitrite: the good, the bad,
679 and the ugly.
680 Koskenkorva T, Aro-Kärkkäinen N, Bachmann D, Arai H, Frey AD, Kallio PT. 2008.
681 Transcriptional activity of Pseudomonas aeruginosa fhp promoter is dependent on two
682 regulators in addition to FhpR. *Arch Microbiol* **189**:385–396. doi:10.1007/s00203-007-0329-
683 3
684 Krichels A, DeLucia EH, Sanford R, Chee-Sanford J, Yang WH. 2019. Historical soil drainage
685 mediates the response of soil greenhouse gas emissions to intense precipitation events.
686 *Biogeochemistry* **142**:425–442. doi:10.1007/s10533-019-00544-x
687 Krichels AH, Yang WH. 2019. Dynamic Controls on Field-Scale Soil Nitrous Oxide Hot Spots
688 and Hot Moments Across a Microtopographic Gradient. *J Geophys Res Biogeosciences*
689 **124**:3618–3634. doi:10.1029/2019JG005224
690 Kuhns DB, Priel DAL, Chu J, Zarember KA. 2015. Isolation and Functional Analysis of Human
691 Neutrophils. *Curr Protoc Immunol* **111**:139–148. doi:10.1002/0471142735.im0723s111
692 Kuypers MMM, Marchant HK, Kartal B. 2018. The microbial nitrogen-cycling network. *Nat Rev*
693 *Microbiol* **16**:263–276. doi:10.1038/nrmicro.2018.9
694 Lilja EE, Johnson DR. 2016. Segregating metabolic processes into different microbial cells
695 accelerates the consumption of inhibitory substrates. *ISME J* **10**:1568–1578.
696 doi:10.1038/ismej.2015.243
697 Lowery NV, Ursell T. 2019. Structured environments fundamentally alter dynamics and stability
698 of ecological communities. *Proc Natl Acad Sci U S A* **116**:379–388.
699 doi:10.1073/pnas.1811887116
700 Lycus P, Bøthun KL, Bergaust L, Shapleigh JP, Bakken LR, Frostegård Å. 2017. Phenotypic
701 and genotypic richness of denitrifiers revealed by a novel isolation strategy. *ISME J*

702 **11**:2219–2232. doi:10.1038/ismej.2017.82
703 Ma L, Cordero OX. 2018. Solving the structure-function puzzle. *Nat Microbiol* **3**:750–751.
704 doi:10.1038/s41564-018-0186-7
705 Meirelles LA, Newman DK. 2018. Both toxic and beneficial effects of pyocyanin contribute to the
706 lifecycle of Pseudomonas aeruginosa. *Mol Microbiol* **110**:995–1010.
707 doi:10.1111/mmi.14132
708 Niehaus L, Boland I, Liu M, Chen K, Fu D, Henckel C, Chaung K, Miranda SE, Dyckman S,
709 Crum M, Dedrick S, Shou W, Momeni B. 2019. Microbial coexistence through chemical-
710 mediated interactions. *Nat Commun* **10**. doi:10.1038/s41467-019-10062-x
711 Pessi IS, Viitamäki S, Eronen-Rasimus E, Delmont TO, Luoto M, Hultman J. 2020. Truncated
712 denitrifiers dominate the denitrification pathway in tundra soil metagenomes. *bioRxiv*.
713 doi:10.1101/2020.12.21.419267
714 Ponomarova O, Patil KR. 2015. Metabolic interactions in microbial communities: Untangling the
715 Gordian knot. *Curr Opin Microbiol* **27**:37–44. doi:10.1016/j.mib.2015.06.014
716 Price-Whelan A, Dietrich LEP, Newman DK. 2007. Pyocyanin alters redox homeostasis and
717 carbon flux through central metabolic pathways in Pseudomonas aeruginosa PA14. *J*
718 *Bacteriol* **189**:6372–6381. doi:10.1128/JB.00505-07
719 Prieto-Barajas CM, Valencia-Cantero E, Santoyo G. 2018. Microbial mat ecosystems: Structure
720 types, functional diversity, and biotechnological application. *Electron J Biotechnol* **31**:48–
721 56. doi:10.1016/j.ejbt.2017.11.001
722 Proctor DM, Relman DA. 2017. The Landscape Ecology and Microbiota of the Human Nose,
723 Mouth, and Throat. *Cell Host Microbe*. doi:10.1016/j.chom.2017.03.011
724 Ratzke C, Barrere J, Gore J. 2020. Strength of species interactions determines biodiversity and
725 stability in microbial communities. *Nat Ecol Evol* **4**:376–383. doi:10.1038/s41559-020-1099-
726 4
727 Rich JJ, Heichen RS, Bottomley PJ, Cromack K, Myrold DD. 2003. Community Composition
728 and Functioning of Denitrifying Bacteria from Adjacent Meadow and Forest Soils. *Appl*
729 *Environ Microbiol* **69**:5974–5982. doi:10.1128/AEM.69.10.5974-5982.2003
730 Richardson DJ. 2000. Bacterial respiration: a flexible process for a changing environment.
731 *Microbiology* **146 (Pt 3**:551–571. doi:10.1099/00221287-146-3-551
732 Sasaki Y, Oguchi H, Kobayashi T, Kusama S, Sugiura R, Moriya K, Hirata T, Yukioka Y, Takaya
733 N, Yajima S, Ito S, Okada K, Ohsawa K, Ikeda H, Takano H, Ueda K, Shoun H. 2016.
734 Nitrogen oxide cycle regulates nitric oxide levels and bacterial cell signaling. *Sci Rep* **6**:1–
735 11. doi:10.1038/srep22038

736 Schindelin J, Arganda-Carreras I, Frise E, Kaynig V, Longair M, Pietzsch T, Preibisch S,
737 Rueden C, Saalfeld S, Schmid B, Tinevez JY, White DJ, Hartenstein V, Eliceiri K,
738 Tomancak P, Cardona A. 2012. Fiji: An open-source platform for biological-image analysis.
739 *Nat Methods* **9**:676–682. doi:10.1038/nmeth.2019
740 Schuster M, Hawkins AC, Harwood CS, Greenberg EP. 2004. The Pseudomonas aeruginosa
741 RpoS regulon and its relationship to quorum sensing. *Mol Microbiol* **51**:973–985.
742 doi:10.1046/j.1365-2958.2003.03886.x
743 Smriga S, Ciccarese D, Babbin AR. 2021. Denitrifying bacteria respond to and shape
744 microscale gradients within particulate matrices. *Commun Biol* **4**:570. doi:10.1038/s42003-
745 021-02102-4
746 Sparacino-Watkins C, Stolz JF, Basu P. 2014. Nitrate and periplasmic nitrate reductases.
747 AUTHOR'S MANUSCRIPT. *Chem Soc Rev* **43**:676–706. doi:10.1039/c3cs60249d.Nitrate
748 Spero MA, Newman DK. 2018. Chlorate Specifically Targets Oxidant-Starved, Antibiotic-
749 Tolerant Populations of Pseudomonas aeruginosa Biofilms Melanie. *MBio* **9**:e01400-18.
750 Stewart PS, Zhang T, Xu R, Pitts B, Walters MC, Roe F, Kikhney J, Moter A. 2016. Reaction-
751 diffusion theory explains hypoxia and heterogeneous growth within microbial biofilms
752 associated with chronic infections. *npj Biofilms Microbiomes* **2**:1–8.
753 doi:10.1038/npjbiofilms.2016.12
754 Tian H, Yang J, Xu R, Lu C, Canadell JG, Davidson EA, Jackson RB, Arneth A, Chang J, Ciais
755 P, Gerber S, Ito A, Joos F, Lienert S, Messina P, Olin S, Pan S, Peng C, Saikawa E,
756 Thompson RL, Vuichard N, Winiwarter W, Zaehle S, Zhang B. 2019. Global soil nitrous
757 oxide emissions since the preindustrial era estimated by an ensemble of terrestrial
758 biosphere models: Magnitude, attribution, and uncertainty. *Glob Chang Biol* **25**:640–659.
759 doi:10.1111/gcb.14514
760 Van Alst NE, Sherrill LA, Iglewski BH, Haidaris CG. 2009. Compensatory periplasmic nitrate
761 reductase activity supports anaerobic growth of Pseudomonas aeruginosa PAO1 in the
762 absence of membrane nitrate reductase. *Can J Microbiol* **55**:1133–1144. doi:10.1139/W09-
763 065
764 VoBwinkel R, Neidt I, Bothe H. 1991. The production and utilization of nitric oxide by a new,
765 denitrifying strain of Pseudomonas aeruginosa. *Arch Microbiol* **156**:62–69.
766 doi:10.1007/BF00418189
767 Volk N., Vollmer D, Schmidt M, Oppermann W, Huber K. 2004. Nitric Oxide, an Old Molecule
768 With Noble Functions in Pseudomonas aeruginosa Biology. *Adv Polym Sci* **166**:29–65.
769 doi:10.1016/j.cossms.2010.07.001

770 Weinstein BT, Lavrentovich MO, Möbius W, Murray AW, Nelson DR. 2017. Genetic drift and
771 selection in many-allele range expansions, bioRxiv. doi:10.1101/145631
772 Widder S, Allen RJ, Pfeiffer T, Curtis TP, Wiuf C, Sloan WT, Cordero OX, Brown SP, Momeni B,
773 Shou W, Kettle H, Flint HJ, Haas AF, Laroche B, Kreft JU, Rainey PB, Freilich S, Schuster
774 S, Milferstedt K, Van Der Meer JR, Grobkopf T, Huisman J, Free A, Picioreanu C, Quince
775 C, Klapper I, Labarthe S, Smets BF, Wang H, Soyer OS, Allison SD, Chong J,
776 Lagomarsino MC, Croze OA, Hamelin J, Harmand J, Hoyle R, Hwa TT, Jin Q, Johnson
777 DR, de Lorenzo V, Mobilia M, Murphy B, Peaudecerf F, Prosser JI, Quinn RA, Ralser M,
778 Smith AG, Steyer JP, Swainston N, Tarnita CE, Trably E, Warren PB, Wilmes P. 2016.
779 Challenges in microbial ecology: Building predictive understanding of community function
780 and dynamics. *ISME J* **10**:2557–2568. doi:10.1038/ismej.2016.45
781 Wilbert SA, Mark Welch JL, Borisy GG. 2020. Spatial Ecology of the Human Tongue Dorsum
782 Microbiome. *Cell Rep* **30**:4003-4015.e3. doi:10.1016/j.celrep.2020.02.097
783 Yoon SS, Karabulut AC, Lipscomb JD, Hennigan RF, Lymar S V., Groce SL, Herr AB, Howell
784 ML, Kiley PJ, Schurr MJ, Gaston B, Choi KH, Schweizer HP, Hassett DJ. 2007. Two-
785 pronged survival strategy for the major cystic fibrosis pathogen, Pseudomonas aeruginosa,
786 lacking the capacity to degrade nitric oxide during anaerobic respiration. *EMBO J* **26**:3662–
787 3672. doi:10.1038/sj.emboj.7601787
788 Yu K, Mitchell C, Xing Y, Magliozzo RS, Bloom BR, Chan J. 1999. Toxicity of nitrogen oxides
789 and related oxidants on mycobacteria: M. tuberculosis is resistant to peroxynitrite anion.
790 *Tuber Lung Dis* **79**:191–198. doi:10.1054/tuld.1998.0203
791 Zhang IH, Mullen S, Ciccarese D, Dumit D, Martocello DE, Toyofuku M, Nomura N, Smriga S,
792 Babbin AR. 2021. Ratio of organic carbon to fixed nitrogen regulates metabolic
793 specialization and denitrification dynamics in Pseudomonas aeruginosa. Front
794 Microbiol 12:1-13. https://doi.org/10.3389/fmicb.2021.711073
795 Zumft WG. 1997. Cell biology and molecular basis of denitrification. *Microbiol Mol Biol Rev*
796 **61**:533–616. doi:10.1128/mmbr.61.4.533-616.1997
797 Zuñiga C, Zaramela L, Zengler K. 2017. Elucidation of complexity and prediction of interactions
798 in microbial communities. *Microb Biotechnol* **10**:1500–1522. doi:10.1111/1751-7915.12855
799
800
801
802

803 **Figure Legends**

804

805 **Figure 1.** Design and characterization of synthetic nitric oxide cross-feeding community. (**A**) WT
806 PA14 denitrification pathway (**B**) Schematic of NO consumer and producer strains where genes
807 that have been deleted are grayed-out, and those remaining are shown in black. The pathway
808 partitions where NO is produced and reduced. (**C**) Growth curve of co-culture 4 members grown
809 individually and together, compared to the WT, over 72hrs under anoxic conditions with nitrate
810 provided as sole terminal electron acceptor (TEA). (**D**) Growth rescue of producer strain using
811 the chemical NO scavenger c-PTIO.

812

813 **Supplemental file 1**. Synthetic NO cross-feeding co-culture comparisons. (**A**) Schematic
814 representation of genomic identity of consumer and producer strains as done Figure 1B. Wiggly
815 arrows indicate intermediates that can be exchanged. (**B**) Growth curves for specified
816 strains/co-cultures.

817

818 **Figure 2.** Patterning of producer and consumer strains under sessile anoxic conditions. (**A**) Phenotypic
819 predictions. (**B**) Representative images showing growth patterns of indicated strain mixtures
820 constitutively expressing either GFP or mApple after anoxic growth for 48hrs under an agar pad with
821 nitrate provided as sole TEA. (**C,D**) Zoom-in of WT mixture showing strains growing as clonal patches
822 (C) compared with zoom-in of the co-culture showing intermixing (**D**). Consumer strain is
823 Δ*narGHJI*Δ*nirS*Δ*napAB*. Producer strain is Δ*norCB*Δ*nosZ*.

824

825 **Supplementary file 2.** Planktonic culture population ratios and sessile aggregate counts. (**A**)
826 Co-culture 4 and 3 were grown as specified for the anoxic growth curves (Figure 1) but with
827 fluorescence constructs to identify the compositional ratio. Co-cultures with the consumer
828 expressing GFP and producer expressing mApple (left two datasets) were compared to the
829 reciprocal cultures with consumer expressing mApple and producer expressing GFP (right two
830 datasets). (**B**) Producer aggregates when grown alone (Pro.) vs. in co-culture with the consumer
831 (Pro. + Con.). (**C**) Consumer aggregates when grown alone (Con.) vs in co-culture with the
832 producer (Con. + Pro.). Consumer strain is Δ*narGHJI*Δ*nirS*Δ*napAB*. Producer strain is
833 Δ*norCB*Δ*nosZ*.

834

835 **Figure 3.** Oxic vs hypoxic growth of planktonic cultures supplemented with and without nitrate. (**A-D**)
836 48hr growth curves cultured under the indicated conditions. Evenly oxygenated environments ("oxic-

837 shaking") were achieved by shaking cultures during incubation (A,B), while unevenly oxygenated
838 environments ("hypoxic-stagnant") were achieved by culturing without shaking (C,D). (**E**) Oxygen
839 profiles from non-shaking cultures of the WT compared to profiles from the co-culture at two time
840 points. (**F,G**) Fluorescent dye readings of superoxide and nitric oxide accumulation over a hypoxic
841 growth curve with nitrate (as in D).
842
843 **Figure 4.** Spatiotemporal patterning of lysis within aggregate biofilms as a function of which nitrate
844 reductase is present. **A**) Transcriptional regulatory control of Nap/Nar gene expression (left).
845 Predictions of spatial Nap and Nar activity in a biofilm, given this regulation (right). Nap can reduce
846 nitrate (NO_3^-) to nitrite (NO_2^-) throughout biofilm, and reduction at the surface prevents nitrate diffusion
847 into the biofilm core. Without Nap, nitrate may penetrate deeper. (**B**) Time lapse of producer (Nap/Nar)
848 biofilm lysis occurring from the periphery inward. (**C**) Time lapse of producer (Nar) biofilm lysis
849 occurring from the core outward. (**D**) At the same time point, three distinct representative biofilms
850 arranged by amount of lysis observed per producer type. Red channel represents CellROX staining
851 indicating presence of superoxide. All images are displayed using the same display settings for direct
852 comparison. (**E**) Schematic interpretation of results. NO leads to superoxide production; superoxide
853 localization correlates with lysis: left represents the dynamic for a Nap/Nar producer, right represents
854 the dynamic for a Nar producer.
855
856 **Supplementary file 3.** Visualization of lysis in a Nap/Nar producer biofilm. High magnification image
857 showing lysis, which is interpreted from a loss of fluorescence and increase in transparency in phase
858 contrast.
859
860 **Figure 5.** Patterning of producer and consumer strains under sessile oxic conditions. (**A**)
861 Representative images of indicated strains grown as biofilms for 24hrs under oxic conditions in the
862 presence of nitrate. (**B**) Zoom-in of WT clonal expansion showing no intermixing. (**C**) Zoom-in of co-
863 culture 4 showing producer survival adjacent to the consumer expansion interface; note that cells
864 appear brightest prior to lysis. (**D**) Three additional high magnification callouts to spotlight specific
865 structural features. (**E**) Time lapse of co-culture 4 showing temporal producer lysis occurring in the
866 absence of consumer contact.
867
868 **Supplemental file 4.** Comparison of patterning of the producer in sessile oxic co-culture (**A**) Producer
869 (Nap/Nar) shows lysis throughout biofilms and when paired with the consumer, regardless of
870 fluorescent identifier; producer shows lysis in the absence of consumer contact. (**B**) Producer (Nar)

871 shows lysis in the center of biofilm, and no significant difference compared to in the presence or
872 absence of the consumer. (**C**) Proposed model in which the Nap/Nar producer and consumer strains
873 both grow clonally until the microenvironment changes such that the producer begins to lyse. The
874 consumer acts as a sink for NO in close proximity to the producer, relieving NO toxicity and preventing
875 lysis.
876
877 **Supplemental Table 1**. Primers, plasmids, cut sites and strains used to make the mutants used in this
878 study.
879
880

Figure 1

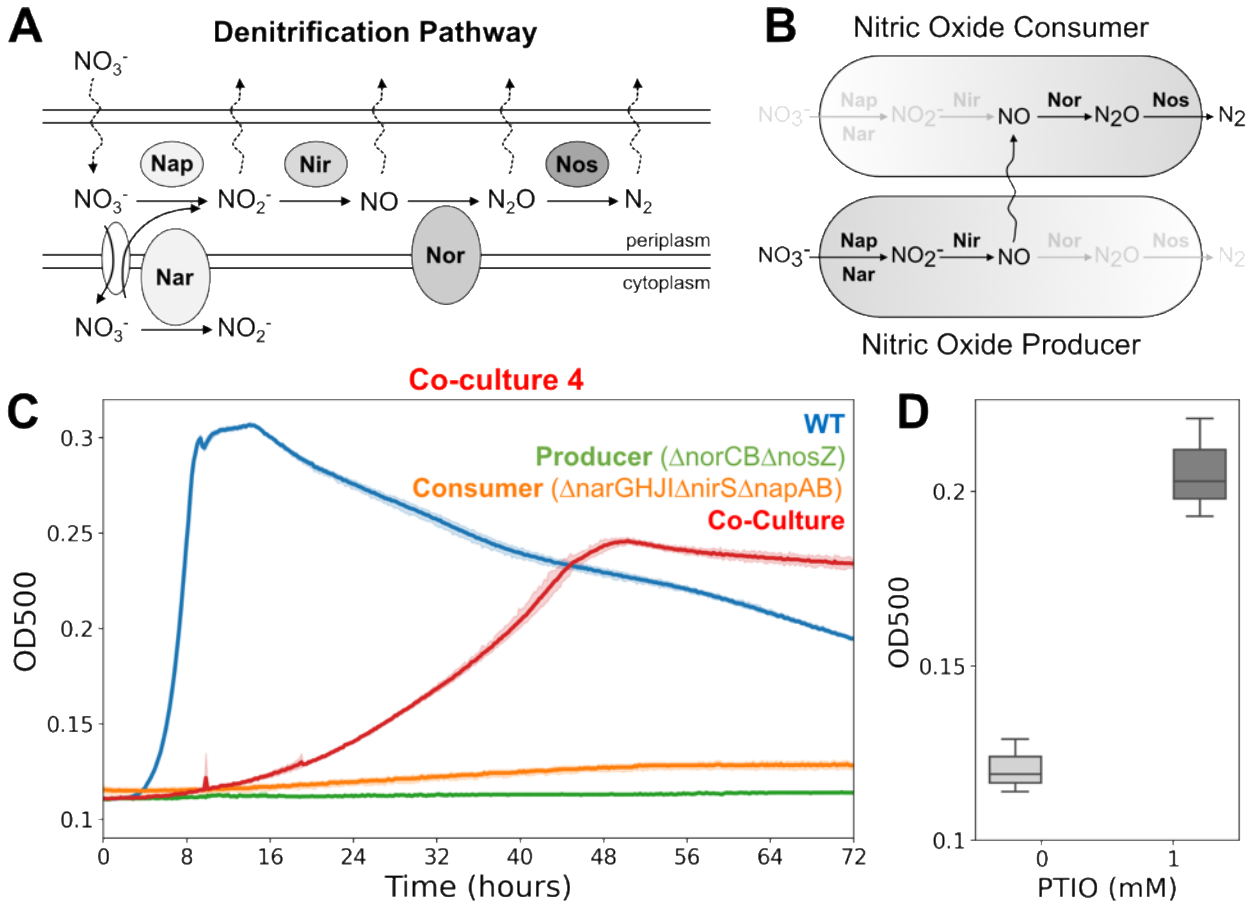
A
Denitrification Pathway
NO3-
Nap
Nir
Nos
NO3-
NO2-
NO
N2O
N2
Nar
Nor
periplasm
cytoplasm
NO3-
NO2-
B
Nitric Oxide Consumer
NO3-
Nap
Nar
NO2-
Nir
NO
Nor
N2O
Nos
N2
NO3-
Nap
Nar
NO2-
Nir
NO
Nor
N2O
Nos
N2
Nitric Oxide Producer
C
Co-culture 4
WT
Producer (ΔnorCBΔnosZ)
Consumer (ΔnarGHJIΔnirSΔnapAB)
Co-Culture
OD500
Time (hours)
D
OD500
PTIO (mM)

Supplementary file 1

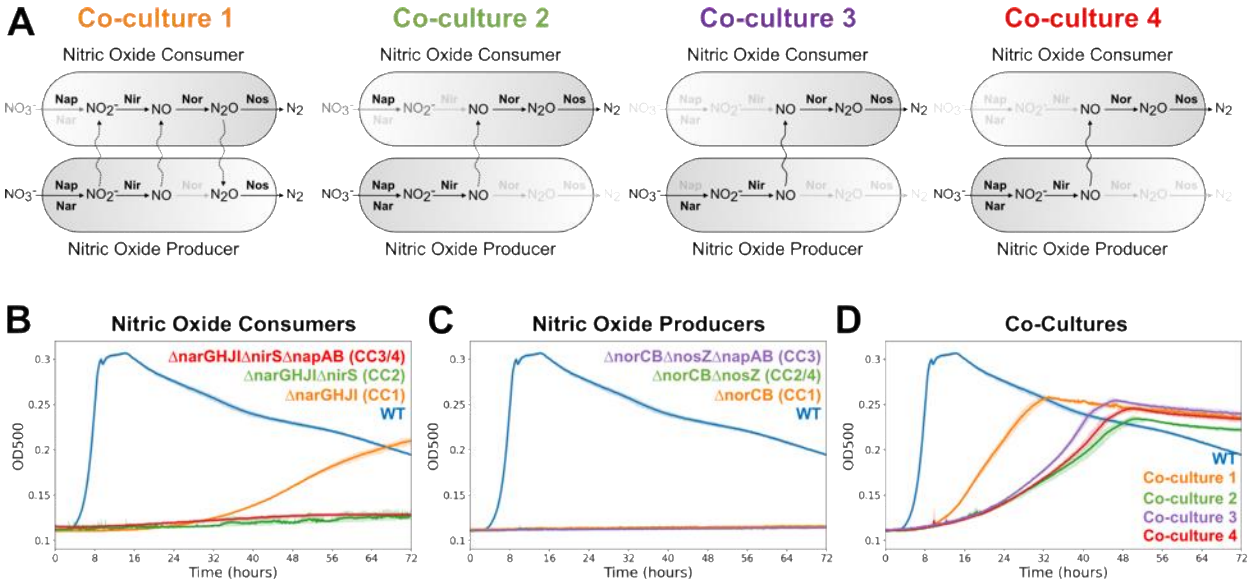

Figure 2

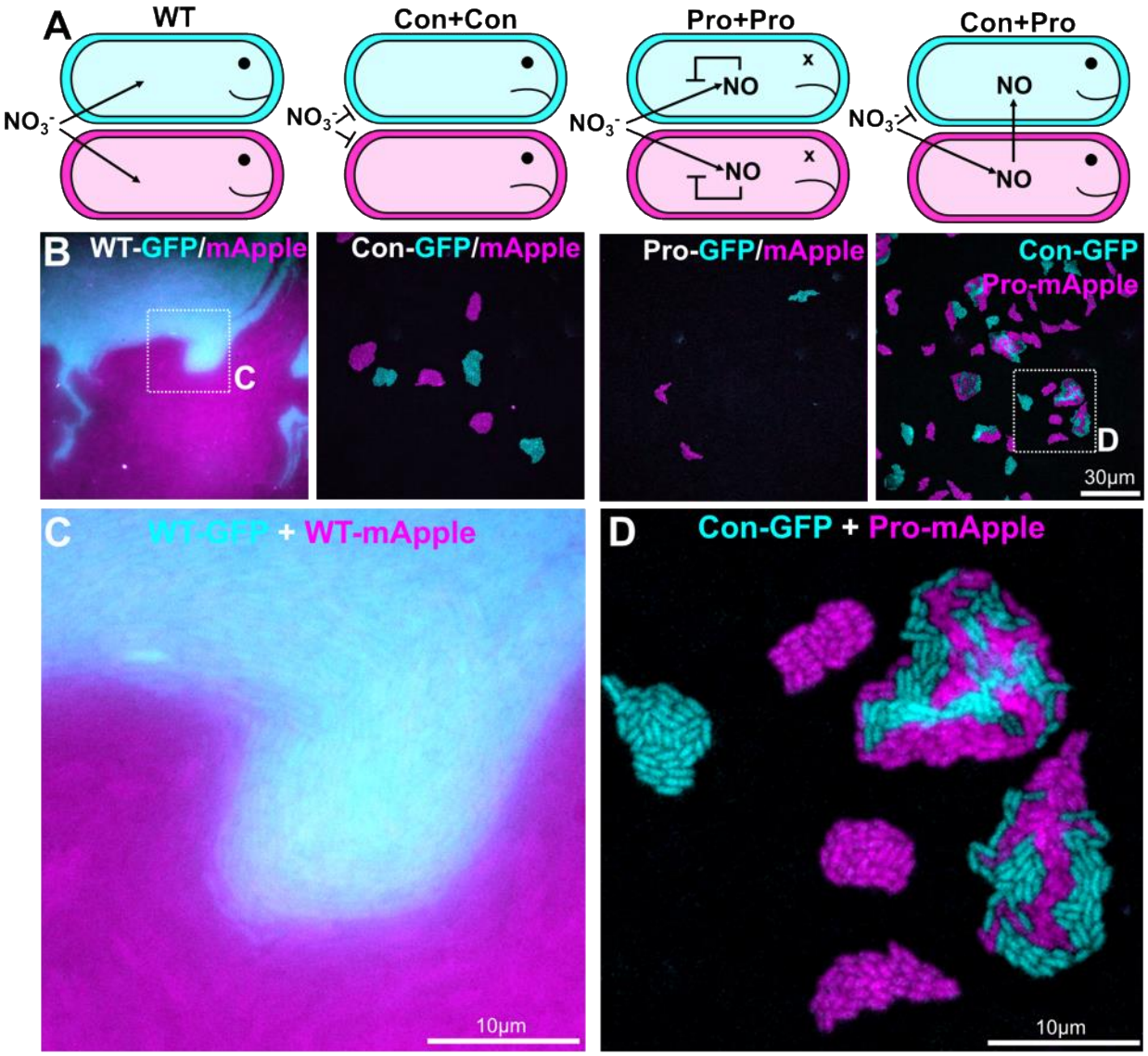
A
WT
Con+Con
Pro+Pro
Con+Pro
NO_3^-
NO
x
B
WT-GFP/mApple
C
Con-GFP/mApple
Pro-GFP/mApple
Con-GFP
Pro-mApple
D
30μm
C
WT-GFP + WT-mApple
10μm
D
Con-GFP + Pro-mApple
10μm

Supplementary file 2

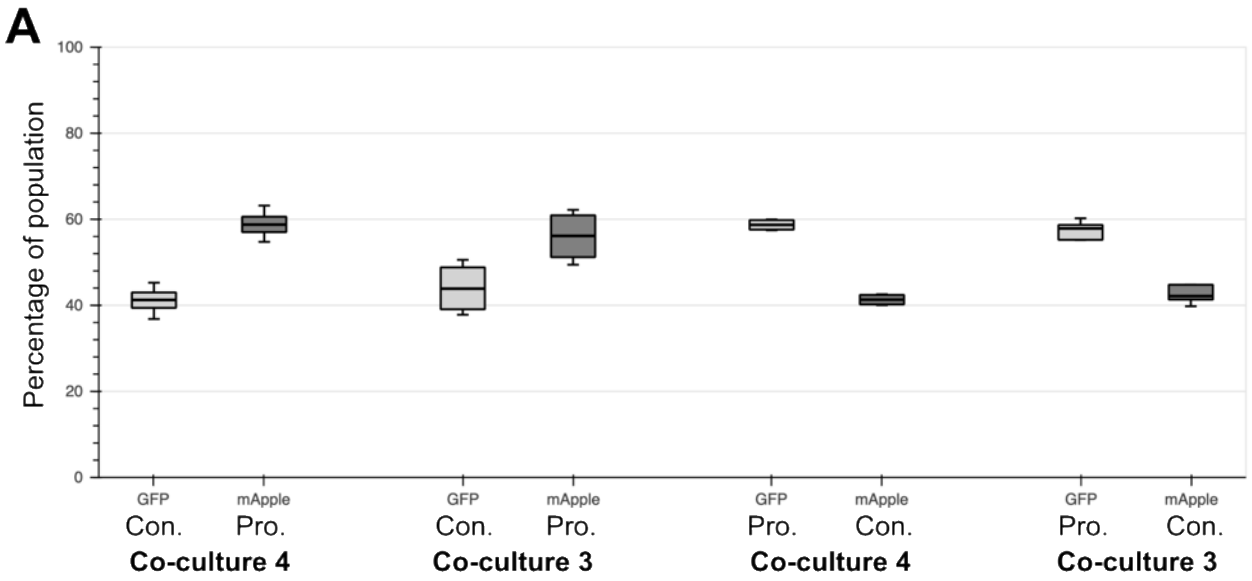

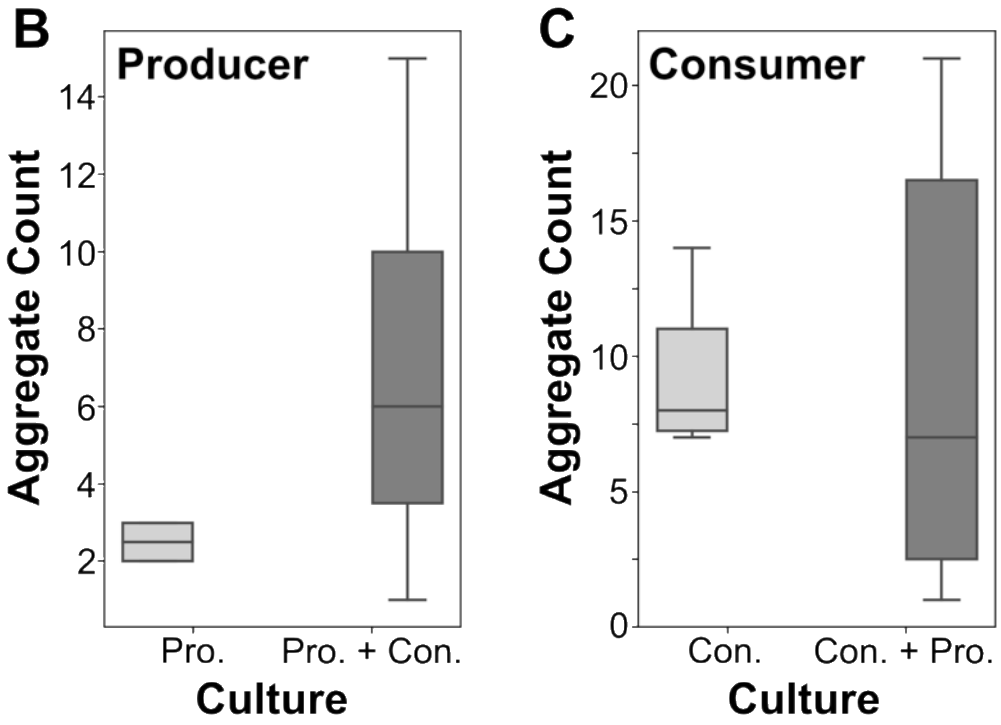

Figure 3

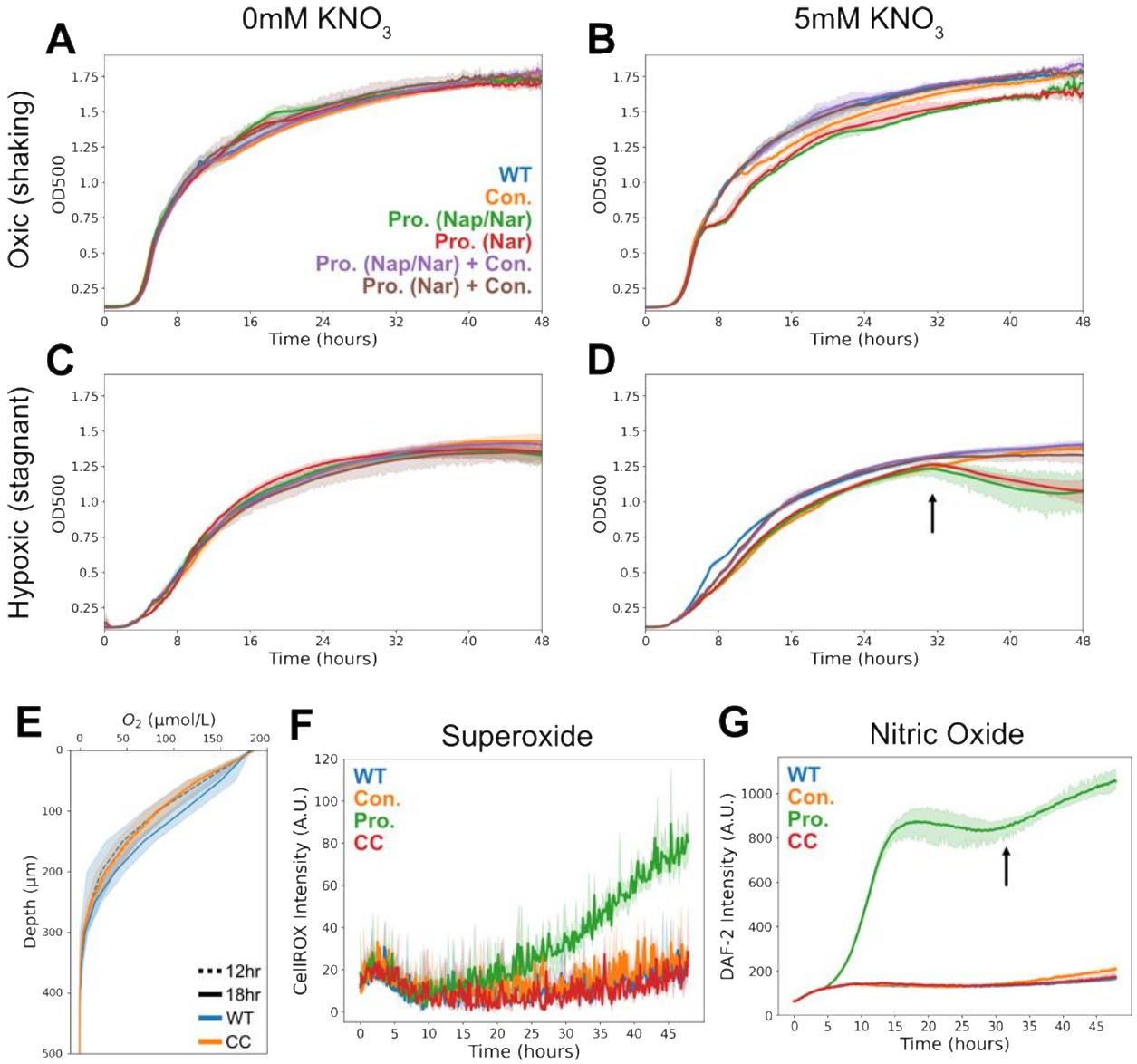
A
0mM KNO3
B
5mM KNO3
Oxic (shaking)
Hypoxic (stagnant)
OD500
Time (hours)
WT
Con.
Pro. (Nap/Nar)
Pro. (Nar)
Pro. (Nap/Nar) + Con.
Pro. (Nar) + Con.
C
D
E
O2 (µmol/L)
Depth (µm)
12hr
18hr
WT
CC
F
Superoxide
CellROX Intensity (A.U.)
WT
Con.
Pro.
CC
G
Nitric Oxide
DAF-2 Intensity (A.U.)

Figure 4

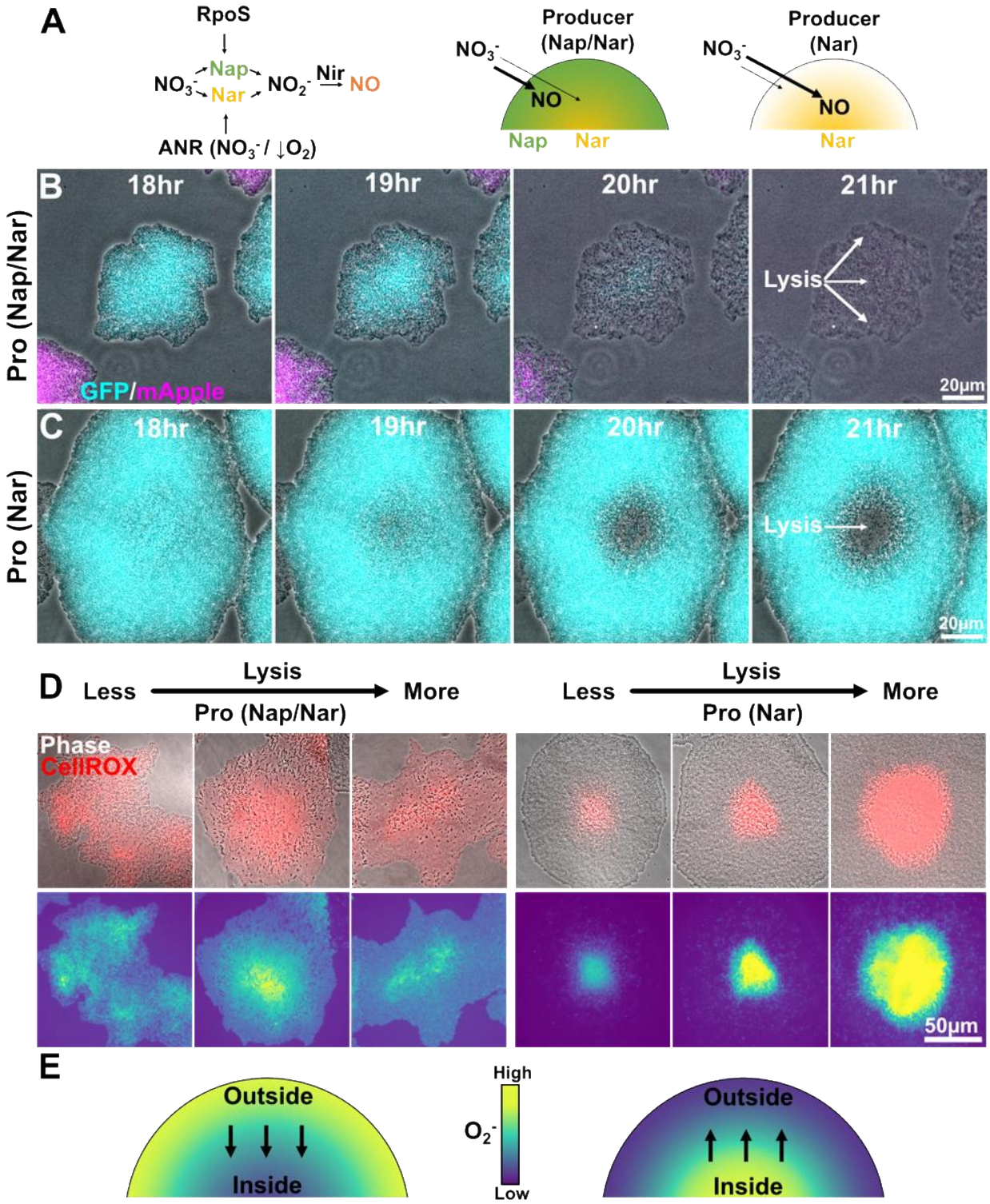
A
RpoS
Nap
Nar
NO_3^-
NO_2^-
Nir
NO
ANR (NO_3^- / ↓O_2)
Producer (Nap/Nar)
Producer (Nar)
NO_3^-
NO
Nap
Nar
B
18hr
19hr
20hr
21hr
Lysis
GFP/mApple
20μm
Pro (Nap/Nar)
C
Pro (Nar)
D
Less
Lysis
More
Pro (Nap/Nar)
Pro (Nar)
Phase
CellROX
50μm
E
Outside
Inside
High
Low
O_2^-

Supplementary file 3

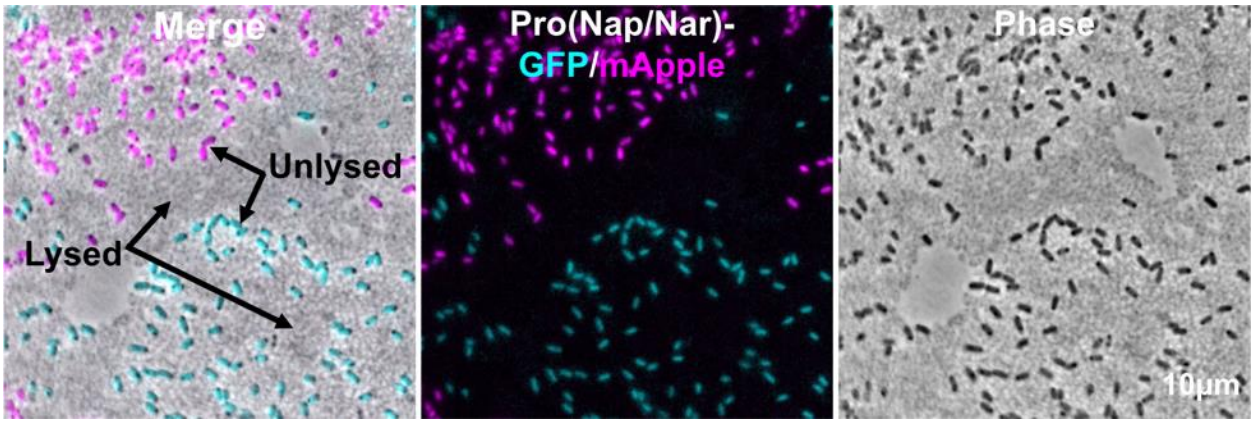

Figure 5

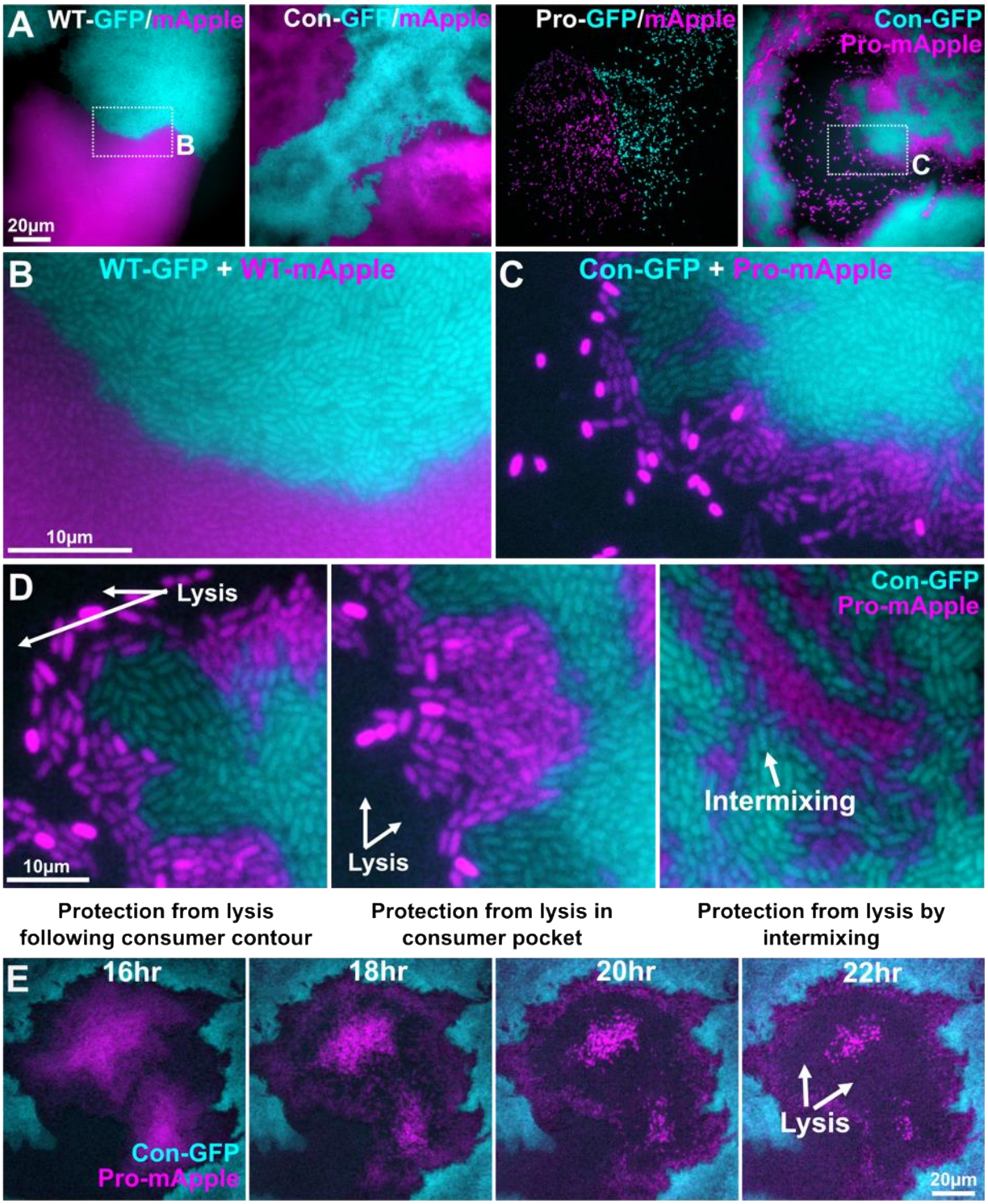
A
WT-GFP/mApple
Con-GFP/mApple
Pro-GFP/mApple
Con-GFP
Pro-mApple
B
C
20μm
B
WT-GFP + WT-mApple
10μm
C
Con-GFP + Pro-mApple
D
Lysis
10μm
Lysis
Con-GFP
Pro-mApple
Intermixing
Protection from lysis following consumer contour
Protection from lysis in consumer pocket
Protection from lysis by intermixing
E
16hr
18hr
20hr
22hr
Con-GFP
Pro-mApple
Lysis
20μm

Supplementary file 4

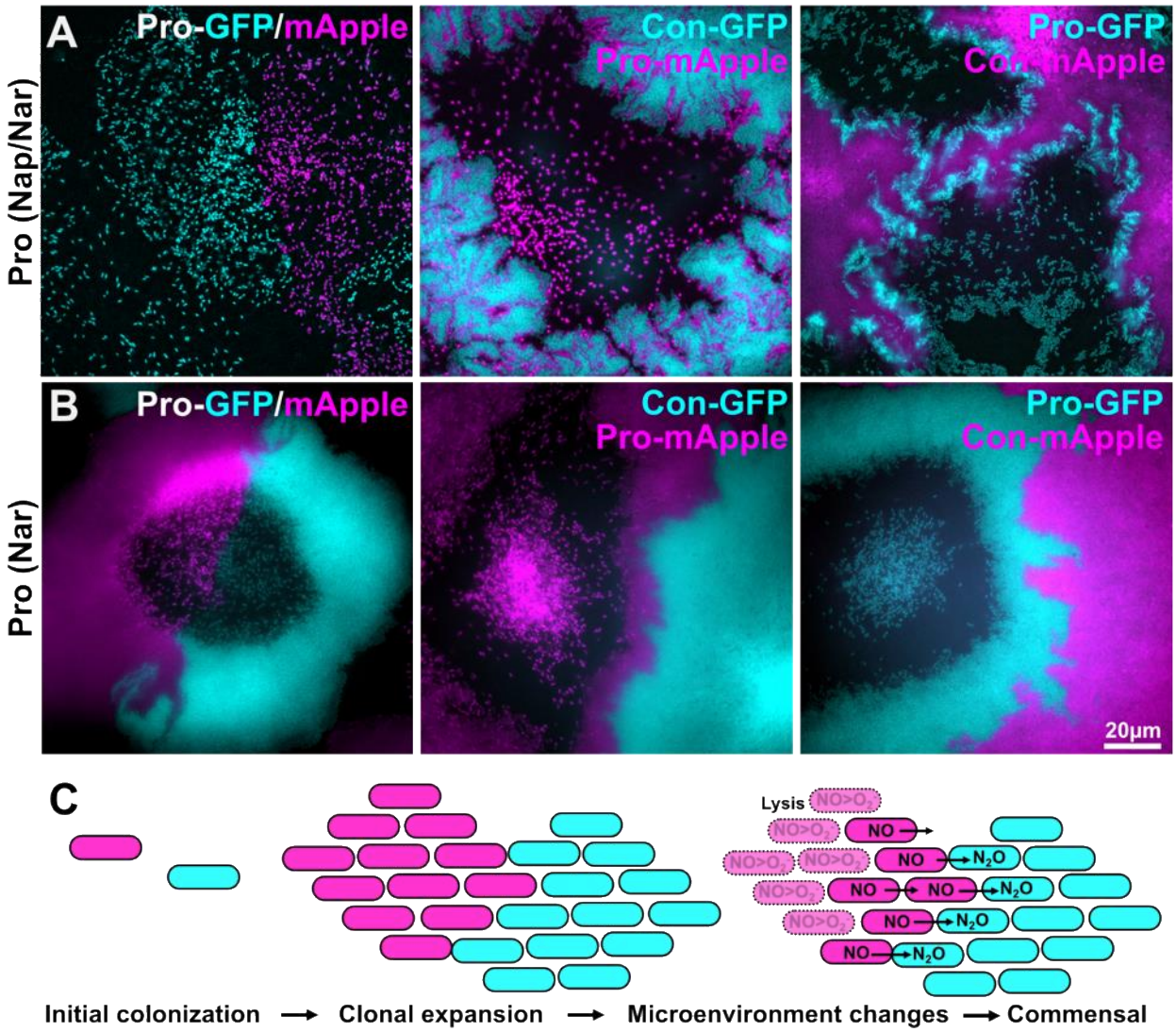

Supplementary Table 1

Deletion Construct	NarGHJI	NapAB	NirS	NorCB	NosZ
Function	Membrane bound nitrate reductase	Periplasmic nitrate reductase	Nitrite reductase	Nitric oxide reductase	Nitrous oxide reductase
Up F	TAAAACGACGGCCAGTGCCACGTACTGGGTGTTCGCCCTG	ACGACGGCCAGTGCCAAGCTTCTACAGTCGCCTGCATAGA	ACGACGGCCAGTGCCAAGCTTGTCGATGCGCTGGGCCAGCA	TAAAACGACGGCCAGTGCCATGATCCTCGGCTGGCTGG	ACGACGGCCAGTGCCAAGCTACGTACTTGACCTGCTGGCG
Up R	CGCGCAGGGTCTTGATCTCCTCACCCGGTC	GTGCTTTCATGCGGCCTCCCCGATTGTCTCCTCGGGCGAG	GGCTCCTGAGGAGATAGACCGACCCGCGTGCGGGGCACGC	GAAGGCCATCGCGGCCTCCTGGAATGGG	GCCCTTGAGGACGACACGAGTCCACTCAGCGCGGTCGATG
Dn F	GGAGATCAAGACCCTGCGCGGCCGGCGCAT	CTCGCCCGAGGAGACAATCGGGGAGGCCGCATGAAAGCACTCA	GCGTGCCCCGCACGCGGGTCGGTCTATCTCCTCAGGAGCC	AGGAGGCCGCGATGGCCTTCGCCGTCGAG	CATCGACCGCGCTGAGTGGACTCGTGTCGTCCTCAAGGGC
Dn R	CATGATTACGAATTCGA GCTGCTGGCGCGGCAGGAAGCGC	CATGATTACGAATTCGAGCTTCCTGCCGACCGGGGCCCAG	CATGATTACGAATTCGAGCTTATCAGGCGACATGGAGATC	CATGATTACGAATTCGAGCTCCGGGCAATCGTCCAGCG	CATGATTACGAATTCGAGCTGAGGAACTGGCCGCCCTGGA
Plasmid	pMQ30	pMQ30	pMQ30	pMQ30	pMQ30
Cut Sites	HindIII, SacI	HindIII, SacI	HindIII, SacI	HindIII, SacI	HindIII, SacI
Published	Spero et al 2018	This study	This study	This study	This study

Strain name	Parent	Deletion	Function of deletion	Published
PA14 (WT)	PA14	NA	NA	NA
ΔnarGHJI	PA14	NarGHJI	Membrane nitrate reductase	Spero et al 2018
ΔnorCB	PA14	NorCB	Nitric oxide reductase	This study
ΔnirS	PA14	NirS	Nitrite reductase	This study
ΔnarGHJIΔnirS	ΔnirS	NarGHJI	Membrane bound nitrate reductase, nitrite reductase	This study
ΔnorCBΔnosZ	ΔnorCB	NosZ	Nitric oxide reductase, nitrous oxide reductase	This study
ΔnarGHJIΔnirSΔnapAB	ΔnarGHJIΔnirS	NapAB	Membrane nitrate reductase, nitrite reductase, periplasmic nitrate reductase	This study
ΔnorCBΔnosZΔnapAB	ΔnorCBΔnosZ	NapAB	Nitric oxide reductase, nitrous oxide reductase, periplasmic nitrate reductase	This study